Haptoglobin and glutamine synthetase may biomark cachexia induced by anti-acute myeloid leukemia chemotherapy

Dean G. Campelj[1,2,3], Cara A. Timpani[1,4,5], Guinevere Spiesberger[1,4], Luke E. Formosa[6], Joel R. Steele[7], Haijian Zhang[7], Ralf B. Schittenhelm[7], Lewis Leow[4,5], Craig A. Goodman[8], Emma Rybalka[1,4,5]*

[1]Institute for Health and Sport, Victoria University, Melbourne, Victoria, 8001, Australia

[2]Biology of Ageing Laboratory, Centre for Healthy Ageing, Centenary Institute, Camperdown, New South Wales, 2050, Australia

[3]Faculty of Medicine and Health, Charles Perkins Centre, University of Sydney, Sydney, 2050, Australia

[4]Inherited and Acquired Myopathies Program, Australian Institute for Musculoskeletal Science, St Albans, Victoria, 3021, Australia

[5]Department of Medicine—Western Health, Melbourne Medical School, The University of Melbourne, St Albans, Victoria, 3021, Australia

[6]Department of Biochemistry and Molecular Biology, Monash Biomedicine Discovery Institute, Monash University, Clayton, Victoria, 3168, Australia

[7]Monash Proteomics and Metabolomics Platform, Department of Biochemistry and Molecular Biology, Monash University, Clayton, Victoria, 3168, Australia

[8]Centre for Muscle Research, and Department of Anatomy and Physiology, The University of Melbourne, Parkville, Victoria, 3010, Australia

*Corresponding author: emma.rybalka@vu.edu.au, +61 3 83958226

Abstract:

Background: Anti-cancer chemotherapy is an underappreciated contributor to cancer cachexia, an often irreversible body wasting condition that causes 20-30% of cancer-related deaths. An obstacle to predicting, monitoring and understanding the mechanisms underlying chemotherapy cachexia is that each cancer (and sub-type) is assigned different chemotherapeutic compounds, typically in multi-agent regimens. Here, we investigate the chemotherapy induction regimen (CIR) used in haematological cancer, acute myeloid leukemia (AML). We hypothesized that the AML CIR would induce cachexia, including loss of lean tissue mass and skeletal muscle atrophy.

Methods: Using an unbiased proteomics approach we interrogated the underlying molecular mechanisms. 3-month-old male Balb/c mice were treated with the AML CIR via intraperitoneal injections of daunorubicin (1.7 mg/kg) on days 1-3, and cytarabine (33.2 mg/kg) administered on days 1-7 or vehicle. Mice were assessed 24 hours after the last treatment, on day 8, or allowed to recover for 2 weeks and assessed on day 22. A third cohort were given access to running wheels in cages. We assessed body composition, whole body metabolism and assessed the muscle proteome using quantitative tandem mass tag labelling LC-MS/MS analysis.

Results: The AML CIR induced acute cachexia involving a ~13% loss of body mass, ~9% loss of lean mass and ~10% reduction in skeletal muscle fibre size. Whole body metabolism and ambulatory activity declined. This cachexic phenotype did not recover over the 2-week post-CIR period (lean mass loss post-CIR: 1-week ~7% vs 2-weeks ~9%). In voluntarily active CIR-treated mice, body wasting was exacerbated due to unchecked loss of fat mass (CIR sedentary: ~31% vs CIR active: ~51%). Muscle proteome studies revealed upregulation of haptoglobin (Hp) and glutamine synthetase (Glul), which were positively correlated with body and lean mass loss. Hp was sensitive to the conditional induction, recovery and exacerbation of AML CIR-mediated cachexia, suggestive of biomarker potential.

Conclusions: The AML CIR induces an acute reduction of body, lean and fat mass underpinned by skeletal muscle atrophy, hypermetabolism and catabolism. Our data uncovered a conditionally sensitive muscle biomarker in Hp, which may be useful as a prognostic tool across other scenarios of chemotherapy-induced myopathy and cachexia or as a target for therapeutic discovery in follow up studies.

Keywords

Anti-cancer chemotherapy, cachexia, skeletal muscle wasting, atrophy, biomarkers, haptoglobin

Introduction:

Cancer-associated cachexia is a multifactorial wasting syndrome involving loss of body and lean tissue mass that may also include fat loss [1]. Common hallmarks of cachexia are skeletal muscle wasting and impaired muscle function, systemic inflammation, dysregulated metabolism and reduced food intake [2]. Cancer cachexia has been historically associated with tumour-host signalling interactions that drive muscle wasting. However anti-cancer chemotherapy has gathered traction as a critical cachexia-promoting factor [3]. In experimental models, chemotherapeutic agents administered as monotherapies, or as part of multi-agent regimens, can induce cachexia in otherwise healthy animals and potentiate cachexic wasting in tumour-burdened animals [4, 5]. In the clinical setting, chemotherapy can promote a vicious wasting cycle involving the loss of skeletal muscle mass which, in turn, impacts patients' response to chemotherapy and increases the risk of dose-related toxicities [6]. Prevalent in ~80% of all cancer patients, cachexia is a substantial factor in cancer-related mortality, as 20-30% of all cancer patients will die directly from cachexia rather than cancer-specific morbidities [7]. While not specific to cancer cachexia, survivors that have endured a critical illness experience can be burdened by muscle-related disability for up to 5 years post and are at high risk of acquiring co-morbidities [8]. These data indicate that whether treated or untreated, cancer patients are prone to skeletal muscle wasting that may debilitate them for life.

Patients with haematological cancers such as acute myeloid leukemia (AML), are prone to cachexia, although the phenomenon is contextually less well studied than with solid tumours of the pancreas, gastro-oesophageal, head and neck, lung and colorectal [2]. Skeletal muscle mass has emerged as a key prognostic factor for survival in AML [9]. Thus, preventing muscle cachexia is critical for improving survival in a disease that already has grim survival statistics [10]. Cachexia in the AML setting may, in part, be driven by the intensity of initial treatment. Universally, this comprises the '7+3' chemotherapy induction regimen (CIR) [10]. The AML CIR incorporates delivery of the anti-metabolite, cytarabine, over 7-days, concomitant with 3-days of an anthracycline, typically daunorubicin or its analogue, idarubicin, on days 1-3. AML patients may receive multiple cycles of the CIR before complete remission is achieved. Thereafter, patients receive consolidation chemotherapy and are assessed for haematopoietic cell transplantation (HCT) eligibility. HCT is the only current curative strategy for AML. Pre-HCT cachexia leads to poor treatment-related outcomes and is a growing area of interest and concern for clinicians [11]. While there are limited data on the impact of daunorubicin and cytarabine on skeletal muscle (or on driving cachexia), other anthracyclines, such as doxorubicin, induce severe cachexia and myopathy [3]. Whether body, lean and muscle mass are recoverable after AML chemotherapy treatment is unknown. However, children with

haematological cancers that receive intense chemotherapy tend to not recover their muscle mass and function from these acute insults, leaving survivors to carry the burden of poor muscle health later in life [12].

The inability to predict those likely to develop muscle cachexia and those who manifest early symptoms is hampering clinical treatment of cancer and other chronic diseases in which cachexia is devastating. In this regard, quantitative proteomics enables the detection of protein biomarkers that become disproportionate relative to the muscle-specific proteome in disease states. These proteins have the potential to not only indicate the likelihood and scope of cachexia impact, but also to predict the likelihood that cachexia could be life-threatening and assess the effectiveness of potential therapeutics. In this study, we sought to identify putative protein biomarkers of cachexia via quantitative tandem mass tag (TMT)-labelling proteomics. We hypothesised, in line with data for the anthracycline analogue, doxorubicin, that the AML CIR would drive cachexia, including skeletal muscle wasting. We identified haptoglobin (Hp) and glutamine synthetase, a.k.a. glutamine/glutamate-ammonia ligase (Glul), as novel biomarkers of muscle wasting due to chemotherapy treatment. We tested the lability of these proteins using voluntary exercise as a physiological stimulus, given the interest in exercise as a protective strategy against cachexia. Our data show that Hp biomarks the extent of especially lean mass loss during treatment, recovery and in response to interventional therapy. An unexpected discovery of our research is that contrary to clinical reports, voluntary exercise promoted chemotherapy-induced cachexia by driving fat loss. Our data highlight that caution must be taken when recommending non-specific exercise activity during the administration of AML chemotherapy.

Methods:

Experimental animals

Three-month old (sexually mature) male Balb/c mice were acquired from the Animal Resource Centre (now Ozgene, Western Australia). This age was selected as Balb/c body mass plateaus at 3-months following a rapid growth phase during the first 8 weeks of life. Sex was controlled for due to muscle phenotype heterogeneity between males and females [13]. Mice were housed on a 12-hour light/dark cycle with *ad libitum* access to food i.e., standard rodent chow and water supply throughout the experimental period. All experimental procedures were approved by the Victoria University Animal Ethics Committee (AEETH17/017) and conformed to the Australian Code of Practice for the Care and Use of Animals for Scientific Purposes.

Experimental protocols and treatments

Chemotherapy

Mice were randomly allocated to treatment groups. Mice received the CIR in separate intraperitoneal injections of daunorubicin (1.7 mg/kg) administered on days 1-3 and cytarabine (33.2 mg/kg) administered on days 1-7 or delivery vehicle (VEH; 0.9% saline) administered on days 1-7 (total *n*=20, 10/group). Daunorubicin dose selection was based on our pilot studies, where the maximum tolerable dose was derived through dose escalation from a commencing dose based on Maral and Jouanne [14]. The cytarabine dose administered is equivalent to the dose utilised in clinical AML treatment [15] adjusted as per FDA guidelines to account for the higher metabolic rate of mice [16]. Throughout the CIR, mice were individually housed in metabolic cages to assess ambulatory and metabolic activity during CIR treatment.

Recovery from chemotherapy

Mice (*n*=48, 8/group) received VEH or CIR treatment, were housed communally (*n*=4-5 per cage) and were assessed for recovery from CIR treatment over time. Experimental endpoints were at 24-hours (day 8), 1-week (day 15) and 2-weeks (day 22) after the final CIR treatment (Fig 5A). There were no interventions in the recovery period. These time-points were selected to evaluate acute recovery of body mass and composition following CIR administration.

Biomarker lability using exercise

VEH and CIR-treated mice were randomly allocated to individual metabolic cages containing a running wheel and to sedentary (SED; locked wheel) or voluntarily active (ACT; unlocked wheel) groups (total *n*=40, 10/group). ACT mice had *ad libitum* access to the running wheel throughout the duration of treatment (Fig 5A). The experimental endpoint was 24 hours after the final chemotherapy treatment (i.e., day 8).

Indirect calorimetry & activity monitoring

To evaluate the impact of the '7+3' CIR on whole-body ambulation and energy expenditure, mice were housed in Promethion Metabolic cages (Sable Systems, LV, USA) for 10 days. The first 3 days were used for acclimatisation, and the next 7 days were considered live-data collection. Real-time data was collected throughout the period, as described by us previously [4]. Ambulatory activity was considered as the summation of the distance covered through both wheel and cage metres for voluntarily active mice, and cage meters for sedentary mice.

Body composition analysis

Echo Magnetic Resonance Imaging (echoMRI) was utilised to assess the effect of the '7+3' CIR on body composition parameters, including lean and fat mass, as previously described [4]. In the first experimental design, live mice were placed into an echoMRI body composition analyzer (EMR-150, Echo Medical Systems, USA) and scanned on day 1 (pre-treatment) and day 8 (post-treatment) of the treatment protocol. In the second experimental design assessing recovery from chemotherapy, live mice were scanned on day 1 (pre-treatment) and on days 8, 15 and 22 of the experiment.

Tissue collection

24 hours after the last CIR treatment on day 7 and live analyses on day 8, mice were deeply anaesthetised via isoflurane (5% induction and 2-3% maintenance). Thereafter, muscles were surgically excised, weighed and snap-frozen for post-hoc analyses, including *extensor digitorum longus* (EDL), *soleus* (SOL), *tibialis anterior* (TA), and *quadriceps* (QD) muscles. TA muscles were prepared for histological assessment.

Histological analyses

Muscle atrophy was assessed via gross weights of all harvested muscles and histologically in the TA using haematoxylin & eosin (H&E) staining. TA muscles were cryopreserved in optimal cutting temperature compound (Sakura Finetek) using liquid nitrogen-cooled isopentane and cryosectioned at 8µm (-18°C, Leica CM1950), mounted and stained. Sections were imaged on a Zeiss Axio Imager Z2 microscope (Carl Zeiss MicroImaging GmbH, Germany) at 20x magnification. Muscle fibre cross-sectional area (CSA) was quantitated using ImageJ software (NIH, USA) and fibre frequency distributions were generated as performed previously [4].

Tandem Mass Tag (TMT)-labelled Proteomics and bioinformatics

Quadriceps samples were prepared and processed for TMT labelling and fractionation as previously described [17]. Liquid chromatography-mass spectrometric (LC-MS) analysis was conducted using an Orbitrap Eclipse Tribrid mass spectrometer (Thermo Scientific, Bremen, Germany) attached to a Nano LC system (Dionex Ultimate 3000 RSLCnano). The experiment was performed with in-house optimised methods at the Monash Proteomics and Metabolomics Platform utilised a data-dependent methodology using real-time search-enabled synchronous precursors selection with MS3 (RTS-SPS-MS3) [18]. Raw data files were analyzed using Sequest within Proteome Discoverer (v2.5.0.400, Thermo Scientific) to obtain protein identifications and their respective

reporter ion intensities using in-house standard parameters. The Mouse SwissProt proteome containing only reviewed sequences (accessed June 2023) was used for protein identification at a 1% false discovery rate alongside a common contaminants database. Reporter ion quantifiers used a unique plus razor with analysis centred on protein groups for shared peptide sequences using all peptides for abundance determination; quantitative values were corrected for stable isotope label impurities according to the manufacturer's values. Bioinformatic data analysis was performed as previously described [17]. A cut-off of the adjusted *p*-value of 0.05 (Benjamini–Hochberg method) and a $\log_2$ fold change of 0.75 was applied to determine significantly regulated proteins in the different pairwise comparisons. We utilized the protein abundance data obtained from the Analyst Suite (TMT-Analyst; https://analyst-suites.org/) [19] and conducted differential pathway analysis using Correlation Adjusted MEan RAnk gene set test (CAMERA)-intensity based analysis within Reactome (v83). Briefly, this method uses limma-based differential analysis on mean protein abundances within pathways across samples with adjusted FDR correction to control for multiple hypothesis testing. This approach enables the detection of alterations in pathways that could remain unobserved when examining only differentially expressed proteins because individual proteins might not provide comprehensive insights into how a specific pathway is changing when assessed through global, untargeted proteomic-level statistical comparisons. The FDR of <0.05 is reported.

Statistics

Data are presented as mean ± standard error of the mean and were statistically analysed with GraphPad Prism (v8, CA, USA) and α set at 0.05. In the first experimental design, data were analysed by t-test (CIR v VEH) or two-way ANOVA (treatment x muscle/tissue) with repeated measures where necessary (fibre size frequency). In the second experimental design, data were analysed by repeated measures two-way ANOVA or mixed-effects analysis. In the third experimental design, two-way ANOVA (with repeated measures where necessary) was used. Tukey's or Bonferroni's post-Hoc testing was used to detect between group effects. Proteomics statistics are stated above. Linear regression correlations were performed on pooled sample sets to determine associations between biomarker proteins (Hp and Glul) and changes in body, lean and fat mass.

Results:

AML CIR induces acute cachexia in mice.

Our first aim was to assess the impact of the AML CIR on body mass and composition, and specifically, muscle wasting in mice. Mice were administered a clinically relevant AML CIR over one week (day 1-7) and

were assessed 24h after the final CIR does on day 8. Body mass decreased by 10% incorporating a ~10% loss of lean and ~30% loss of fat mass between the pre- and post-treatment assessments Fig. 1A). Body wasting could not be entirely explained by reduced caloric intake since the slight reduction of mean food intake in CIR mice was not statistically significant (Fig. 1B). Mass of the EDL, SOL and TA muscles was also reduced (Fig. 1C). However, when corrected for body mass, there was no effect of CIR (Supp Table 1), highlighting that muscle wasting is proportionate to the overall loss of body mass, rather than exclusively targeted by chemotherapy. As per muscle, CIR reduced the mass of all organs assessed (diaphragm, heart, spleen, kidneys, epi fat and liver (Fig. 1C)). In summary, our data show AML CIR induces >5% loss of body mass, involving loss of both muscle and fat mass, fitting the clinical definition of cachexia.

Next, we used histology to investigate the impact of AML CIR at the muscle architectural level. The fibre size distribution of TA muscles revealed CIR induced muscle fibre atrophy (Fig. 1D). There were significantly more smaller fibres with a cross-sectional area (CSA) between 800-1400 mm^2 and fewer larger fibres ranging from 2800-3600 mm^2 (Fig. 1D). Overall, CIR reduced the mean fibre CSA by ~20% (Fig. 1D). To determine whether fibre size shifts were due to phenotype transformations or traditional atrophy signalling, we probed our TMT-labelled proteomics data set (performed in quadriceps muscle) for fibre type-specific myosin heavy chain (MyH) isoforms in addition to the atrophy biomarkers, Atrogin-1/F-box only protein 32 (Fbxo32), E3 ubiquitin-protein ligase, muscle RING-finger protein-1 (MuRF-1/Trim63), and components of the inducible transforming growth factor β (Tgfbi)/myostatin (Mstn)/suppressor of mothers against decapentaplegic (Smad) axis (Fig. 1E). There was significant upregulation (based on false discovery rate (FDR) from pathways enrichment) of fast-twitch fibre-specific MyH isoforms, Myh1 and Myl, as well as of atrophy regulator, Atrogin-1, indicating that fast-type fibre transformations may attempt to compensate for global fibre atrophy (Fig. 1E). Since anthracyclines are known to cause oxidative stress which may lead to muscle damage, we also assessed TA cross-sections for signs of histopathology. There was no evidence of active muscle necrosis or regeneration that would indicate CIR-induced damage, e.g., signs of damaged feathered fibres, inflammatory infiltrate, centronucleated fibres and myotubes (Fig. 1D) nor was there evidence of fibrosis as determined by picrosirius staining (Fig. 1F).

AML CIR reduces physical activity and systemic energy expenditure.

Throughout the treatment period, mice were housed in Promethion® metabolic cages with activity tracking capability. Relative to cage metres travelled on day 1, CIR mice reduced their physical activity levels from day 3 of treatment and maintained significantly lower levels for the duration of the treatment period compared to VEH

mice (Fig. 2A). Interestingly, energy expenditure only decreased from day 4 of treatment, indicating a 24 h window where energy expenditure is increased relative to physical activity levels (Fig. 2B). However, when endpoint energy expenditure was corrected for lean tissue mass, there was no difference between VEH and CIR-treated mice (Fig. 2C). Our data indicate that energy expenditure is dependent on lean tissue mass and physical activity may reduce to conserve both. Since both fat and lean mass catabolism was implicated in CIR induced body wasting (Figure 1), we calculated the respiratory quotient (RQ; VCO_2/O_2), a marker of preferential substrate utilisation and shifts thereof. The RQ showed a significant shift in fat relative to carbohydrate metabolism in CIR mice at day 7 (Fig. 2D).

Hp and Glul are responsive to AML CIR induced muscle cachexia.

To better understand the molecular response leading to muscle wasting induced by AML CIR, we performed quantitative TMT-labelling proteomics to identify differentially expressed proteins as potential biomarkers of chemotherapy cachexia. Of the 4,716 proteins that were detected, only Hp and Glul were observed to be differentially expressed in response to AML CIR treatment according to the cut-off criteria ($\log_2$ 0.75-fold change, adjusted *p* value=0.05), and both were upregulated (Fig. 3A & B). Five additional proteins were different based on adjusted *p* (0.05) only: Acad11 (acyl-coA dehydrogenase family member 11), Ca14 (carbonic anhydrase 14), Cd36 (platelet glycoprotein 4/fatty acid translocase/scavenger receptor class B member 3) and Plin4 (perilipin 4) were upregulated, while Dgkz (diacylglycerol kinase zeta) was downregulated. Pathways enrichment was performed on the entire data set using Reactome to uncover the underlying molecular response. Of the 12 pathways that were significantly upregulated in response to AML CIR (listed in order of most to least significant based on FDR; Fig. 3C), all were involved in mitochondrial metabolism of amino acid, glycolytic and fatty acid substrates. The most significantly dysregulated pathway was branched chain amino acid (BCAA) catabolism, consistent with the loss of muscle mass observed based on mass and histological atrophy. We deeply probed the BCAA pathway as well as β-fat oxidation and mitochondrial tricarboxylic acid (TCA) cycle pathways, to decipher the mechanisms underlying CIR-induced body wasting (Fig. 3D). Of the 18 proteins within the BCAA catabolism pathway our proteomics detected, CIR upregulated 14 (78%). The most significantly upregulated protein was branched chain keto acid dehydrogenase E1 subunit a (Bckdha), an inner mitochondrial protein involved in catabolism of leucine, isoleucine and valine. In fact, most of the 14 upregulated BCAA proteins were involved in catabolism of either valine or leucine. There were 47 β-fat oxidation related proteins captured in our proteome and 27 were upregulated (57%) by AML CIR treatment. Notably, almost all family members of acyl-coA

dehydrogenase (Acad), an enzyme involved in the metabolism of acyl-coA variants, were upregulated (as was Acad6A1 in the BCAA pathways). Acad11 was the most significantly upregulated protein within the β-fat oxidation pathway. Several protein subunits of the mitochondrial TCA cycle were upregulated (aconitase (Aco2), isocitrate dehydrogenase (Idh1), malate dehydrogenase (Mdh2) and succinate dehydrogenase (Sdhaf1)) although notably the TCA pacesetter and mitobiogenesis biomarker, citrate synthase (Cs), was not. Our data suggest a remodelling of mitochondria to drive BCAA (especially valine and iso-/leucine) and fat oxidation. Since anthracyclines are metabolised by mitochondrial Complex I, we also probed this pathway. Specific components of NADH-ubiquinone oxidoreductase (Nduf) were upregulated, including core subunit V2 (Ndufv2), which is known to protect against doxorubicin-induced mitochondrial dysfunction driven cardiomyopathy [20]. Uncoupling-related proteins were also probed as a potential mechanism of hypermetabolism (Fig. 3E). Uncoupling proteins 1 and 3 (Ucp1, 3) were both upregulated in CIR relative to VEH muscle although Ucp1 was more highly expressed than Ucp3 indicating thermogenesis as a mechanism.

One hundred and thirty-five Reactome pathways were downregulated in CIR versus VEH muscle (Supp Table 2) and the top 25 pathways are presented in Fig. 3F. Many of the downregulated pathways were associated with ribosomal protein translation and synthesis and the topmost downregulated pathway (based on FDR from pathways enrichment) was inflammation-dependent (via tumor necrosis factor receptor 1 (Tnfr1) ceramide production). In fact, several pathways concerning inflammation regulator, nuclear factor kappa B (Nf-κb) activity were reduced. Of note, the macroautophagy pathway, which when conditionally up- or down-regulated can induce muscle atrophy [21], was significantly downregulated. Collectively, our data indicate that muscle protein synthesis pathways are suppressed, and catabolism is increased to provide substrates for mitochondrial metabolism.

Fat, but not lean mass, recovers in the two weeks following AML CIR.

To test the ability of the body, lean and fat mass to recover after chemotherapy treatment, we next treated a cohort of mice with the same AML CIR then allowed them to recover for two weeks during which body mass was recorded daily and body composition assessed weekly (Fig. 4A). Body mass was lowest at day 9 (~80% of starting body mass at day 2 of recovery and 48 h after the last chemotherapy dose) and began to recover from day 10 (Fig. 4B). However, by the end of the 2-week recovery period, body mass had not fully recovered and remained at 90-95% of the starting body mass. Body mass displacement from the VEH group was greatest at day 8 and least at day 22 of recovery, but there was no significant difference between assessment timepoints in the CIR group (Fig. 4C). Body mass did not recover sufficiently to renounce the clinical definition of cachexia. Lean mass was more

resistant to recovery than fat mass. While fat mass displacement from VEH was still statistically different at day 22 of recovery, it did partially recover between day 8 and 22 by ~50%, whereas lean mass displacement did not shift (Fig. 4C). There was no recovery of EDL, SOL or TA muscle mass observed (Fig. 4D). The muscle proteome was also resistant to change – there was no significant change in muscle Hp and Glul expression at day 22 based on log-fold change and adjusted *p* value post-recovery (Fig. 4E). However, there were shifts in quadriceps Hp expression for individual animals indicating Hp is responsive to withdrawal of CIR and may biomark early changes in molecular signalling within muscle (Fig. 4E). In contrast, Glul was non-responsive to CIR withdrawal (Fig. 4E).

Voluntary exercise during AML CIR treatment worsens cachexia and further upregulates Hp.

There is great interest in exercise as a protective modality for cachexia [22]. Thus, we included additional cohorts of VEH and AML CIR treated mice with *ad libitum* voluntary access to running wheels (ACT) over the 7-day AML CIR to test (1) the consequences of wheel-running during chemotherapy administration and (2) the lability of Hp and Glul as cachexia biomarkers. On average, VEH ACT mice covered ~100x more distance on the running wheel compared to ground metres covered by VEH SED mice, while CIR ACT mice covered ~60x more than CIR SED mice (data not shown). From day 3 of treatment, CIR ACT mice became steadily less active (ground and wheel metres) with endpoint physical activity <50% of starting activity levels relative to VEH ACT (Fig. 5A). Energy expenditure reduced proportionate to ambulatory distance, although notably, was reduced from day 2 of treatment (Fig. 5B). In healthy VEH mice, food intake increased to match the additional energy expenditure from increased physical activity (Fig. 5C) sufficient to resist changes in body mass (Fig 5D). However, although CIR ACT mice were 60x more physically active than CIR SED counterparts, food consumption was not increased to meet energy expenditure (Fig. 5B and C). While incremental changes in body and lean mass were too small to be statistically different, there was a trend for CIR ACT mice to lose both body and lean tissue mass (significant CIR group effects were found), whereas VEH ACT mice tended to reduce body mass but increase lean mass (Fig. 5D). The most significant effect of increased physical activity was on fat mass. VEH ACT mice lost ~30% of their pre-ACT fat mass, whereas CIR ACT mice lost ~50%. At the muscle level, CIR ACT mice had very different responses to exercise compared to VEH ACT mice where the predominantly fast-twitch glycolytic type 2 EDL muscle increased in size but the predominantly slow-twitch oxidative type 1 SOL did not change (Table 1). In contrast, in WT ACT mice, the EDL mass did not shift but the SOL mass increased (Table 1). There was no effect

of exercise on mass (Table 1) or mean fibre size (Fig. 5E) of the mixed fibre type TA muscle in either VEH or CIR treated mice.

Physical activity induced a unique proteomic signature (shifts in 10 of the 4,766 proteins detected) in VEH mouse quadriceps involving upregulation of heat shock (Hsp1a, Hsp1b, Hsp90aa1, Hsph1, Hspb1, Cryab), DNA repair (Rad21), muscle regeneration (Tubb6), and fatty acid metabolism (Fabp5, Nudt7) proteins (Fig. 5F). Relative to VEH ACT, the CIR ACT proteome was considerably more impacted with 40 dysregulated proteins detected (13 upregulated, 27 downregulated). The most upregulated protein was Hp, which was 6.8-fold higher than VEH following exercise exposure (i.e., CIR ACT v VEH ACT) compared with 5.8-fold higher in sedentary mice (i.e., CIR SED v VEH SED). Other upregulated proteins included those associated with slow fibre isoform (Myoz2, Myl3, Myh7b)), extracellular matrix remodelling (Serpina3m), muscle regeneration (Apcs), and energy metabolism (Pdk4, Lrrc2, Slmap, CGfpt2, Aacs, Plin5). Downregulated proteins were associated with reduced immunogenicity/inflammation (C8g, C8a, C8b, C9, H2Ab1), endoplasmic reticulum proliferation (Rrbp1), collagen biosynthesis (P4ha1, Rcn3, Serpinh1), and polyamine (Smox), fatty acid and cholesterol biosynthesis (Aac) indicative of a whole cell wasting phenotype. Notably, Ucp1 expression was normalised and Ucp3 expression was downregulated by exercise. Muscle Glul expression was not different in the AML CIR ACT relative to the VEH ACT group.

Interrogating Hp and Glul as biomarkers of cachexia induced by AML CIR.

Biomarkers are useful as predictive, diagnostic and prognostic tools in disease management [23]. Our data demonstrate Hp as the most responsive and labile muscle protein to AML CIR treatment of the >4,700 detected within our proteome (Fig. 6A). Hp's scaled heatmap signature for all conditions expressed relative to VEH SED best reflected the scope of cachexia seen across our experimental conditions, where expression was highest under conditions that caused the biggest mean reduction in body, lean, fat and muscle mass (Fig. 6A). However, only moderate-weak correlations were observed between Hp and each of body and lean mass loss from pre- to post-treatment and there was no correlation with fat mass loss (Fig. 6B). Hp better correlated with lean mass (r^2=0.458, p=0.0004; red points and regression line) when the recovery readouts were removed (denoted by red dots and regression line) indicating it might be a better predictor of CIR-specific molecular pathology and associated muscle mass. There was a weak correlation between Hp expression and endpoint raw quadriceps mass (matched for the same muscle used for proteomics) when recovery data points were removed. Glul expression was less responsive to treatment than Hp, failing to respond to CIR withdrawal during the recovery period or the added

stress of exercise on top of CIR. Glul expression actually increased in VEH quadriceps over the 2-week recovery period and due to physical activity consistent with growth- and physical activity-related metabolism increases. . Glul was strongly correlated (when recovery data were removed, moderately correlated with all data included) with body mass, moderately correlated with lean mass, and weakly correlated with fat mass change from pre-post treatment indicating its expression is relative to the overall metabolic state based on body mass. Glu expression did not correlate with endpoint muscle mass. CIR-induced heatmap signatures of atrophy mediators, Fbxo32 (Atrogin-1) and Trim63 (Murf-1), mimicked the expression pattern of Hp but not Glul, suggesting Hp sensitively detects atrophy signalling.

Discussion:

Haematological cancers, such as AML, are rarely studied in the context of cachexia due to the rapid turnaround from diagnosis to initiation of chemotherapy treatment and evaluation for hematopoietic stem cell transplantation. Given the systemic nature of the cancer, the initial chemotherapy regimen(s) is/are gruelling and the scope for severe chemotherapy-induced myopathy and cachexia is profound. Previously, Amrute-Nayak *et al.* demonstrated *in vitro* that daunorubicin, but not cytarabine treatment disrupted sarcomeric organization and compromised contractility by driving loss of MyH isoforms in primary mouse myotubes [24]. But aside from this study, data on the impact of the AML regimen on skeletal muscle, particularly *in vivo* and in therapeutically relevant dosing regimens, is lacking. We reveal that despite only lasting one week, the AML CIR induces a remarkable level of cachexia involving all the definitive hallmarks [1]. We show an acute reduction of body, lean and fat mass underpinned by skeletal muscle atrophy, hypermetabolism and muscle catabolism. Mice appear to self-execute a tissue preservation mechanism by lowering physical activity and energy expenditure to reduce the catabolic insult. The same response is obvious in humans and termed “the sickness response” [25]. In the context of clinical AML management, this finding alone suggests a need for prevention strategies to be carefully considered [25]. That CIR-induced cachexia persisted at 2 weeks post-delivery where muscles were particularly stubborn to recover, and this was exacerbated in mice exposed to voluntary wheel running, highlights post-treatment muscle recovery therapies are warranted but that exercise recommendations for cancer patients require intensive safety studies.

Persistent hypercatabolism of muscle with reduced energy expenditure was curious to us but there were mechanistic clues within our proteomics screen. Upregulation of Glul, an enzyme that removes ammonia from the muscle purine nucleotide cycle during conversion of glutamate to glutamine, was a distinct outcome of CIR

treatment in our study. Glutamine is also released from muscle tissue during proteolysis [26]. Glul$^{-/-}$ mKO (muscle specific knock-out) mice highlight a critical role for Glul in clearing ammonia, and nitrogen waste product urea and ultimately supporting the hypothesis that muscle glutamine levels are dependent on proteolysis levels [27]. Cytarabine metabolism generates significant ammonia via deamination, which, in addition to increased mitochondrial metabolism, appears to necessitate more Glul as an adaptive response [28]. Whether this response is sufficient to offset CIR-induced ammonia production is unclear. In addition to cytarabine effects, anthracyclines are metabolised by Complex I of the mitochondrial electron transport chain and we speculated that Complex I proteins might be upregulated to effectively process the daunorubicin load. Our proteome-wide pathways analysis revealed upregulation of core NADH-ubiquinone oxidoreductase sub-units, especially subunit V2 (Ndufv2), which was previously shown in the context of doxorubicin treatment previously, to reduce cardiomyopathy [20] caused by mitochondrial dysfunction. We also showed upregulation of Ucp 1 and 3, which drive heat over energy (and CO_2) production explaining why catabolism increased while energy expenditure (measured via respirometry) reduced. It is difficult to differentiate whether mitochondrial uncoupling is fundamentally important to limit oxidative stress linked to daunorubicin metabolism by Complex I or a thermogenesis-related mechanism is activated as fat mass reduces and physical activity levels decline. In the latter scenario, mitochondrial uncoupling likely predicates an increased propensity for hypothermia. Our data suggest that a consequence of these mitochondrial adaptations to CIR metabolism is inadvertent systemic hypermetabolism resulting in muscle catabolism. While likely rare, a fulminant version of the wasting phenotype described has been observed in cancer patients with acute leukemia and coined chemotherapy-related acute rhabdomyolysis [29]. Defending the skeletal muscle BCAA pool from chemotherapy-induced ubiquitylation of L-Type amino acid transporter 1 (LAT1) is a promising approach recently explored *in vitro* [30] and may be useful in the context of the AML '7+3' CIR. This mechanism may link back to upregulated Glul, whereby a futile increase in skeletal muscle glutamine exchange for BCAAs is facilitated by LAT1.

Through unbiased proteomic profiling of quadriceps muscle, we reveal two potential novel biomarkers of AML CIR-induced cachexia, in Hp and Glul. Hp was positively correlated with loss of body and lean mass specifically and highly responsive to conditional induction, recovery and exacerbation of AML CIR-mediated cachexia. Under normal physiological conditions, Hp is synthesised by the liver in response to erythrocyte degradation and circulated in the plasma as an acute-phase protein where it detoxifies free haemoglobin [31]. Hp's role in skeletal muscle is poorly understood. It is difficult to differentiate from our analysis whether it was specifically overexpressed in skeletal muscle or had diffused from the plasma into the muscle extracellular space.

Data from Zip14 metal transporter ablated mice suggests that muscle level expression is sensitive to inflammation-induced stress response signalling [32] indicating the former scenario is likely given Hp expression was highest when heat-shock proteins were also upregulated, i.e., with voluntary wheel running. Positive associations between systemic Hp levels and muscle health have been observed. In humans, plasma Hp is higher in atrophy resistant subjects exposed to 10 days of unloading and lower in cachexic cancer patients [33]. However, Massart *et al.* demonstrated increased skeletal muscle Hp expression in the C26-adenocarcinoma induced cachexia model [34] consistent with our data. Interestingly, Hp abundance is unaffected by Atrogin-1- and Murf-1-dependent immobilisation-atrophy suggesting that its accumulation is invoked by a specific insult to skeletal muscle homeostasis [35]. Bertaggia *et al.* demonstrated increased oxidative stress-associated protein carbonylation in $Hp^{-/-}$ KO mice with muscle atrophy, underpinned by increased Atrogin-1 and Murf-1 mRNA expression, exercise intolerance and muscle weakness, indicating that Hp is redox sensitive [36]. Our data adds to this idea that muscle specific Hp expression patterns mimic mitochondrial stress levels and iron accumulation, a hallmark of doxorubicin induced cardiotoxicity [37]. Our pathways analysis showed upregulated iron sulfur cluster biogenesis in support of this concept. That Hp levels were reducing in some mice by the end of the post-CIR recovery period indicates it's sensitivity to the effects of chemotherapy on muscle. Further investigation is required to validate the connection between chemotherapy-induced Hp accumulation in skeletal muscle, oxidative stress and dysregulated iron metabolism. In contrast to Hp, Glul was positively correlated with each of body, lean and fat mass but was unresponsive to conditional recovery or exacerbation of CIR-induced cachexia by exercise. It appears to biomark overall metabolism, but not CIR-induced hypercatabolism specifically. Further evaluation of these proteins as predictive and/or prognostic biomarkers of cachexia involving muscle wasting are warranted. While a useful biomarker would typically be detectable in easily accessible biofluids (i.e., blood, urine), there is opportunity for muscle specific biomarkers to be clinically useful across cancer treatment, especially for AML where surgical procedures such as bone marrow biopsy and venous port placement/removal/replacement before, during and after chemotherapy treatment, enable access to muscle biopsy. We cannot rule out that muscle Hp is secreted into the bloodstream which would make it a particularly useful biofluid marker of cachexia. This aspect requires further study since there is conjecture between circulating and muscle-specific Hp expression in the context of cachexia. There is no evidence that Glul is secreted from muscle. However, plasma glutamate/glutamine ratios may predict muscle Glul activity and the cachexia hypercatabolic state.

A surprising finding in our study was that exercise exacerbated cachexia by driving further fat mass loss and there was no beneficial recovery of lean tissue to indicate therapeutic value. We saw shifts in muscle mass in fast-

twitch but not slow-twitch muscles with CIR treatment, which directly opposed exercise effects observed in VEH mice, indicating that mitochondria-dense slow twitch fibres may be predominantly affected by CIR combined with the specific muscle activation pattern used in wheel running. Exercise, did, however, reduce Ucp1 and Ucp3 expression suggesting that over the longer term, it may be useful to abate hypermetabolism if mitochondrial uncoupling is the primary cause. Exercise is generally positively associated with muscle mass, function and metabolism and is being explored as a strategic approach to prevent cachexia [22]. Our data indicate the modality and potentially, the intensity, of exercise selected for cancer patients while they are being actively treated is an important consideration in view of the chemotherapeutic agents used. Previously, Wehrle *et al*. compared endurance and resistance training application during chemotherapy induction in 22 (of 29, 24% dropout) acute leukemia patients and demonstrated that only resistance training improved knee extension strength whereas endurance and no training reduced it [38]. The study did not measure body composition nor report on whether any participants were, or became, cachexic. In breast cancer patients undergoing chemotherapy treatment, 12 weeks of aerobic exercise (walking) reduced body and fat mass like our study, although notably, cachexia is not so much a problem in this malignancy [39]. To ensure safe prescription of exercise during AML treatment, more high-quality randomised controlled trials the MENAC (Multimodal-Exercise, Nutrition and Anti-inflammatory medication for Cachexia) trial [40] (Clinical Trials ID: NCT02330926) are necessary. This trial has reported some acute success for weight stabilization in advanced cancer patients undergoing non-curative anti-cancer treatment, with further insights expected to be revealed.

Conclusions:

Overall, our study demonstrates the physiological characteristics of an AML CIR cachexia mouse model and illuminates hypermetabolism of BCAAs and fat as drivers of chemotherapy-induced cachexia through metabolic rewiring of muscle and mitochondrial uncoupling. We identified two potential muscle-specific protein biomarkers in Hp and Glul that could be developed as prognostic tools to monitor efficacy of interventional therapeutics against cachexia. Validation studies are necessary to map time to muscle, lean tissue and body mass recovery as Hp and Glul expression declines, opening up the opportunity to explore divergent responses to AML CIR. Our two-week recovery time point was insufficient in this regard. Future studies characterising the CIR-induced phenotype would benefit from: 1) a longer recovery time course to establish when, or if lean, fat and body mass recovers; 2) multiple CIR dosing after short recovery periods to assess the impact of multiple CIR cycles as is often used in the clinic; and 3) daily muscle and blood sampling across the week-long AML CIR to tease out the

contributions of each of daunorubicin and cytarabine to muscle proteome changes. There is particular interest on day 4, when daunorubicin administration is completed and measurement of transient muscle degradation markers may provide improved sensitivity. Our data also illuminate potential therapeutic avenues against hypermetabolism in the metabolic pathways surrounding Hp (iron metabolism), Glul (urea processing and glutamate/glutamine metabolism) and mitochondrial uncoupling for follow-up.

Acknowledgements:

The authors acknowledge the AML patients who inspired this work and grant support from the Institute for Health and Sport, Victoria University to DGC. This study used BPA-enabled (Bioplatforms Australia)/NCRIS-enabled (National Collaborative Research Infrastructure Strategy) infrastructure located at the Monash Proteomics and Metabolomics Platform.

Ethical standards:

Animal studies were approved by the Victoria University Animal Ethics Committee (AEETH17/017) and conformed to the Australian Code of Practice for the Care and Use of Animals for Scientific Purposes.

Conflict of interest:

ER has received consultancy fees and speaker honoraria from Santhera Pharmaceutical and Epirium Bio outside of this work. The authors declare no conflicts of interest.

References:

1. Fearon K, Strasser F, Anker SD, Bosaeus I, Bruera E, Fainsinger RL, et al. Definition and classification of cancer cachexia: an international consensus. Lancet Oncol. 2011;12:489-95. doi:10.1016/s1470-2045(10)70218-7
2. Baracos VE, Martin L, Korc M, Guttridge DC, Fearon KCH. Cancer-associated cachexia. Nat Rev Dis Primers. 2018;4:17105. doi:10.1038/nrdp.2017.105
3. Campelj DG, Goodman CA, Rybalka E. Chemotherapy-Induced Myopathy: The Dark Side of the Cachexia Sphere. Cancers (Basel). 2021;13:doi:10.3390/cancers13143615
4. Campelj DG, Timpani CA, Petersen AC, Hayes A, Goodman CA, Rybalka E. The Paradoxical Effect of PARP Inhibitor BGP-15 on Irinotecan-Induced Cachexia and Skeletal Muscle Dysfunction. Cancers (Basel). 2020;12:doi:10.3390/cancers12123810
5. Beltrà M, Pöllänen N, Fornelli C, Tonttila K, Hsu MY, Zampieri S, et al. NAD(+) repletion with niacin counteracts cancer cachexia. Nat Commun. 2023;14:1849. doi:10.1038/s41467-023-37595-6
6. Bozzetti F. Forcing the vicious circle: sarcopenia increases toxicity, decreases response to chemotherapy and worsens with chemotherapy. Ann Oncol. 2017;28:2107-18. doi:10.1093/annonc/mdx271
7. Vaughan VC, Martin P, Lewandowski PA. Cancer cachexia: impact, mechanisms and emerging treatments. J Cachexia Sarcopenia Muscle. 2013;4:95-109. doi:10.1007/s13539-012-0087-1

8. Friedrich O, Reid MB, Van den Berghe G, Vanhorebeek I, Hermans G, Rich MM, Larsson L. The Sick and the Weak: Neuropathies/Myopathies in the Critically Ill. Physiol Rev. 2015;95:1025-109. doi:10.1152/physrev.00028.2014
9. Nakamura N, Ninomiya S, Matsumoto T, Nakamura H, Kitagawa J, Shiraki M, et al. Prognostic impact of skeletal muscle assessed by computed tomography in patients with acute myeloid leukemia. Ann Hematol. 2019;98:351-9. doi:10.1007/s00277-018-3508-1
10. Short NJ, Rytting ME, Cortes JE. Acute myeloid leukaemia. Lancet. 2018;392:593-606. doi:10.1016/s0140-6736(18)31041-9
11. Loh KP, Dunne RF, Friedberg JW, Mohile SG. Integrating Assessment of Sarcopenia into Decision-making for Allogeneic Hematopoietic Cell Transplantation: Ready for Prime Time? J Natl Cancer Inst. 2019;111:757-9. doi:10.1093/jnci/djy233
12. Goodenough CG, Partin RE, Ness KK. Skeletal Muscle and Childhood Cancer: Where are we now and where we go from here. Aging Cancer. 2021;2:13-35. doi:10.1002/aac2.12027
13. Rosa-Caldwell ME, Greene NP. Muscle metabolism and atrophy: let's talk about sex. Biol Sex Differ. 2019;10:43. doi:10.1186/s13293-019-0257-3
14. Maral RJ, Jouanne M. Toxicology of daunorubicin in animals and man. Cancer Treat Rep. 1981;65 Suppl 4:9-18.
15. Ellison RR HJ, Weil M, Jacquillat C, Boiron M, Bernard J, Sawitsky A, Rosner F, Gussoff B, Silver RT, Karanas A, Cuttner J, Spurr CL, Hayes DM, Blom J, Leone LA, Haurani F, Kyle R, Hutchison JL, Forcier RJ, Moon JH. Arabinosyl cytosine: a useful agent in the treatment of acute leukemia in adults. Blood. 1968;32:507-23. doi:10.1182/blood-2016-06-725101
16. Nair AB, Jacob S. A simple practice guide for dose conversion between animals and human. J Basic Clin Pharm. 2016;7:27-31. doi:10.4103/0976-0105.177703
17. Timpani CA, Debrincat D, Kourakis S, Boyer R, Formosa LE, Steele JR, et al. Loss of endogenous estrogen alters mitochondrial metabolism and muscle clock-related protein Rbm20 in female mdx mice. Faseb j. 2024;38:e23718. doi:10.1096/fj.202400329R
18. Schweppe DK, Eng JK, Yu Q, Bailey D, Rad R, Navarrete-Perea J, et al. Full-Featured, Real-Time Database Searching Platform Enables Fast and Accurate Multiplexed Quantitative Proteomics. J Proteome Res. 2020;19:2026-34. doi:10.1021/acs.jproteome.9b00860
19. Shah AD, Goode RJA, Huang C, Powell DR, Schittenhelm RB. LFQ-Analyst: An Easy-To-Use Interactive Web Platform To Analyze and Visualize Label-Free Proteomics Data Preprocessed with MaxQuant. Journal of Proteome Research. 2020;19:204-11. doi:10.1021/acs.jproteome.9b00496
20. Yang M, Abudureyimu M, Wang X, Zhou Y, Zhang Y, Ren J. PHB2 ameliorates Doxorubicin-induced cardiomyopathy through interaction with NDUFV2 and restoration of mitochondrial complex I function. Redox Biol. 2023;65:102812. doi:10.1016/j.redox.2023.102812
21. Masiero E, Agatea L, Mammucari C, Blaauw B, Loro E, Komatsu M, et al. Autophagy is required to maintain muscle mass. Cell Metab. 2009;10:507-15. doi:10.1016/j.cmet.2009.10.008
22. Tsitkanou S, Murach KA, Washington TA, Greene NP. Exercise Counteracts the Deleterious Effects of Cancer Cachexia. Cancers (Basel). 2022;14:doi:10.3390/cancers14102512
23. Califf RM. Biomarker definitions and their applications. Exp Biol Med (Maywood). 2018;243:213-21. doi:10.1177/1535370217750088
24. Amrute-Nayak M, Pegoli G, Holler T, Lopez-Davila AJ, Lanzuolo C, Nayak A. Chemotherapy triggers cachexia by deregulating synergetic function of histone-modifying enzymes. J Cachexia Sarcopenia Muscle. 2021;12:159-76. doi:10.1002/jcsm.12645
25. Campelj DG, Timpani CA, Rybalka E. Cachectic muscle wasting in acute myeloid leukaemia: a sleeping giant with dire clinical consequences. J Cachexia Sarcopenia Muscle. 2022;13:42-54. doi:10.1002/jcsm.12880
26. Chang TW, Goldberg AL. The metabolic fates of amino acids and the formation of glutamine in skeletal muscle. J Biol Chem. 1978;253:3685-93.
27. He Y, Hakvoort TBM, Köhler SE, Vermeulen JLM, de Waart DR, de Theije C, et al. Glutamine synthetase in muscle is required for glutamine production during fasting and extrahepatic ammonia detoxification. J Biol Chem. 2010;285:9516-24. doi:10.1074/jbc.M109.092429
28. Park MR, Lee HJ, Jang HM, Kim NH, Lee JS, Jeong YT, et al. Cytarabine induces cachexia with lipid malabsorption via zippering the junctions of lacteal in murine small intestine. J Lipid Res. 2023;64:100387. doi:10.1016/j.jlr.2023.100387
29. Truica CI, Frankel SR. Acute rhabdomyolysis as a complication of cytarabine chemotherapy for acute myeloid leukemia: case report and review of literature. Am J Hematol. 2002;70:320-3. doi:10.1002/ajh.10152
30. Mora S, Adegoke OAJ. Maintenance of the branched-chain amino acid transporter LAT1 counteracts myotube atrophy following chemotherapy. Am J Physiol Cell Physiol. 2024;326:C866-c79. doi:10.1152/ajpcell.00537.2023

31. di Masi A, De Simone G, Ciaccio C, D'Orso S, Coletta M, Ascenzi P. Haptoglobin: From hemoglobin scavenging to human health. Mol Aspects Med. 2020;73:100851. doi:10.1016/j.mam.2020.100851
32. Kim J, Aydemir TB, Jimenez-Rondan FR, Ruggiero CH, Kim MH, Cousins RJ. Deletion of metal transporter Zip14 (Slc39a14) produces skeletal muscle wasting, endotoxemia, Mef2c activation and induction of miR-675 and Hspb7. Sci Rep. 2020;10:4050. doi:10.1038/s41598-020-61059-2
33. Murgia M, Brocca L, Monti E, Franchi MV, Zwiebel M, Steigerwald S, et al. Plasma proteome profiling of healthy subjects undergoing bed rest reveals unloading-dependent changes linked to muscle atrophy. J Cachexia Sarcopenia Muscle. 2023;14:439-51. doi:10.1002/jcsm.13146
34. Massart IS, Paulissen G, Loumaye A, Lause P, Pötgens SA, Thibaut MM, et al. Marked Increased Production of Acute Phase Reactants by Skeletal Muscle during Cancer Cachexia. Cancers (Basel). 2020;12:doi:10.3390/cancers12113221
35. Lin KH, Wilson GM, Blanco R, Steinert ND, Zhu WG, Coon JJ, Hornberger TA. A deep analysis of the proteomic and phosphoproteomic alterations that occur in skeletal muscle after the onset of immobilization. J Physiol. 2021;599:2887-906. doi:10.1113/jp281071
36. Bertaggia E, Scabia G, Dalise S, Lo Verso F, Santini F, Vitti P, et al. Haptoglobin is required to prevent oxidative stress and muscle atrophy. PLoS One. 2014;9:e100745. doi:10.1371/journal.pone.0100745
37. Ichikawa Y, Ghanefar M, Bayeva M, Wu R, Khechaduri A, Naga Prasad SV, et al. Cardiotoxicity of doxorubicin is mediated through mitochondrial iron accumulation. J Clin Invest. 2014;124:617-30. doi:10.1172/jci72931
38. Wehrle A, Kneis S, Dickhuth HH, Gollhofer A, Bertz H. Endurance and resistance training in patients with acute leukemia undergoing induction chemotherapy-a randomized pilot study. Support Care Cancer. 2019;27:1071-9. doi:10.1007/s00520-018-4396-6
39. Kim JJ, Shin YA, Suk MH. Effect of a 12-week walking exercise program on body composition and immune cell count in patients with breast cancer who are undergoing chemotherapy. J Exerc Nutrition Biochem. 2015;19:255-62. doi:10.5717/jenb.2015.15092812
40. Solheim TS, Laird BJA, Balstad TR, Bye A, Stene G, Baracos V, et al. Cancer cachexia: rationale for the MENAC (Multimodal-Exercise, Nutrition and Anti-inflammatory medication for Cachexia) trial. BMJ Support Palliat Care. 2018;8:258-65. doi:10.1136/bmjspcare-2017-001440

Tables:

Table 1. Response of muscle mass to voluntary exercise during acute myeloid leukemia (AML) chemotherapy induction regimen (CIR). Data are mean delta % change active (ACT) relative to sedentary (SED) ± SEM. EDL: extensor digitorum longus; SOL: soleus; TA: tibialis anterior. Variance are. *p<0.05, ****p<0.0001.

	Δ % change VEH ACT v SED	Δ % change CIR ACT v SED
EDL	5.75 ± 3.03	40.41 ± 6.54****
SOL	14.99 ± 3.12	0.44 ± 5.79*
TA	1.93 ± 2.74	-2.26 ± 1.37

Supplemental tables:

Supplemental Table 1: Muscle and organ mass/body mass (mg/g) ratios. Data are mean ± SEM.

	VEH	CIR
Muscles		
Extensor Digitorum Longus (EDL)	0.419 ± 0.007	0.451 ± 0.011
Soleus (SOL)	0.299 ± 0.013	0.307 ±0.010
Tibialis Anteriot (TA)	1.787 ± 0.029	1.903 ± 0.025
Tissues/Organs		
Diaphragm (DIA)	2.834 ± 0.151	3.421 ± 0.185
Heart (HRT)	4.718 ± 0.128	4.742 ± 0.103
Spleen (SPLN)	3.206 ± 0.118	2.421 ± 0.059
Kidney (KID)	7.655 ± 0.149	7.201 ± 0.165
Epidydimal Fat (EPI)	19.340 ± 1.466	18.065 ± 0.624
Liver (LIV)	48.088 ± 2.057	45.781 ± 1.630

Supplemental Table 2: All significantly up- and downregulated Reactome pathways.

Pathway	Direction	Number of Proteins Mapped	FDR
TNFR1-mediated ceramide production	Down	95	1.647E-17
Formation of a pool of free 40S subunits	Down	163	1.314E-12
Eukaryotic Translation Termination	Down	143	1.713E-12
GTP hydrolysis and joining of the 60S ribosomal subunit	Down	188	1.394E-11
Selenocysteine synthesis	Down	140	1.394E-11
L13a-mediated translational silencing of Ceruloplasmin expression	Down	201	1.430E-11
Peptide chain elongation	Down	145	1.501E-11
Eukaryotic Translation Initiation	Down	213	3.495E-11
Cap-dependent Translation Initiation	Down	213	3.495E-11

Nonsense Mediated Decay (NMD) independent of the Exon Junction Complex (EJC)	Down	181	3.495E-11
SRP-dependent cotranslational protein targeting to membrane	Down	168	7.502E-11
Viral mRNA Translation	Down	156	1.456E-10
Eukaryotic Translation Elongation	Down	160	1.487E-10
Response of EIF2AK4 (GCN2) to amino acid deficiency	Down	185	3.864E-10
Selenoamino acid metabolism	Down	183	1.778E-08
Nonsense-Mediated Decay (NMD)	Down	229	2.274E-08
Nonsense Mediated Decay (NMD) enhanced by the Exon Junction Complex (EJC)	Down	229	2.274E-08
Formation of the ternary complex, and subsequently, the 43S complex	Down	113	1.360E-07
Regulation of expression of SLITs and ROBOs	Down	344	1.370E-07
Major pathway of rRNA processing in the nucleolus and cytosol	Down	246	1.425E-07
rRNA processing in the nucleus and cytosol	Down	254	3.020E-07
Translation initiation complex formation	Down	145	7.466E-07
Ribosomal scanning and start codon recognition	Down	130	1.279E-06
Activation of the mRNA upon binding of the cap-binding complex and eIFs, and subsequent binding to 43S	Down	148	1.518E-06
rRNA processing	Down	276	5.877E-06
Cellular response to starvation	Down	243	1.191E-05
Branched-chain amino acid catabolism	Up	36	4.275E-05
SARS-CoV-1 modulates host translation machinery	Down	110	6.946E-05
Signalling by ROBO receptors	Down	526	1.615E-04
Nuclear Receptor transcription pathway	Down	251	3.248E-04
Transcription of SARS-CoV-2 sgRNAs	Down	107	4.676E-04
Influenza Viral RNA Transcription and Replication	Down	282	5.100E-04

RHO GTPases regulate CFTR trafficking	Down	533	5.555E-04
RUNX1 regulates transcription of genes involved in WNT signalling	Down	191	5.635E-04
Defective CFTR causes cystic fibrosis	Down	676	9.779E-04
RUNX1 regulates estrogen receptor mediated transcription	Down	198	1.018E-03
SARS-CoV-2 modulates host translation machinery	Down	104	1.124E-03
Regulation of RUNX2 expression and activity	Down	409	1.187E-03
Cross-presentation of soluble exogenous antigens (endosomes)	Down	111	1.315E-03
NIK-->noncanonical NF-kB signalling	Down	230	2.342E-03
Regulation of ornithine decarboxylase (ODC)	Down	109	2.342E-03
ABC transporter disorders	Down	699	2.396E-03
Translation	Down	468	2.411E-03
SARS-CoV-2 Genome Replication and Transcription	Down	142	2.525E-03
Dectin-1 mediated noncanonical NF-kB signalling	Down	249	2.889E-03
ABC-family proteins mediated transport	Down	712	3.035E-03
Mitochondrial protein import	Up	156	3.462E-03
Influenza Infection	Down	386	4.032E-03
Autodegradation of the E3 ubiquitin ligase COP1	Down	226	4.659E-03
The citric acid (TCA) cycle and respiratory electron transport	Up	304	4.783E-03
Oxygen-dependent proline hydroxylation of Hypoxia-inducible Factor Alpha	Down	199	4.979E-03
Citric acid cycle (TCA cycle)	Up	35	5.600E-03
Metabolism of polyamines	Down	128	6.683E-03
SUMOylation of intracellular receptors	Down	285	6.683E-03
Stabilization of p53	Down	249	7.596E-03
Late endosomal microautophagy	Down	710	7.664E-03

Nef-mediates down modulation of cell surface receptors by recruiting them to clathrin adapters	Down	69	8.453E-03
G1/S DNA Damage Checkpoints	Down	275	8.925E-03
Ub-specific processing proteases	Down	1018	8.925E-03
TNFR1-induced NF-kappa-B signaling pathway	Down	345	8.925E-03
Transcriptional regulation by RUNX2	Down	595	8.925E-03
Clathrin-mediated endocytosis	Down	959	8.925E-03
Disorders of transmembrane transporters	Down	772	8.925E-03
Cargo recognition for clathrin-mediated endocytosis	Down	902	8.925E-03
Beta-oxidation of pristanoyl-CoA	Up	9	9.366E-03
Cellular response to hypoxia	Down	223	9.366E-03
Vif-mediated degradation of APOBEC3G	Down	172	9.366E-03
Aggrephagy	Down	742	9.423E-03
p53-Dependent G1 DNA Damage Response	Down	271	9.423E-03
p53-Dependent G1/S DNA damage checkpoint	Down	271	9.423E-03
Autodegradation of Cdh1 by Cdh1:APC/C	Down	161	9.423E-03
Ovarian tumor domain proteases	Down	442	9.423E-03
Constitutive Signalling by Aberrant PI3K in Cancer	Down	444	9.423E-03
FBXL7 down-regulates AURKA during mitotic entry and in early mitosis	Down	192	1.012E-02
Mitochondrial Fatty Acid Beta-Oxidation	Up	61	1.012E-02
Regulation of RUNX3 expression and activity	Down	217	1.012E-02
Mitochondrial iron-sulfur cluster biogenesis	Up	39	1.012E-02
TFAP2 (AP-2) family regulates transcription of growth factors and their receptors	Down	350	1.012E-02
Ubiquitin Mediated Degradation of Phosphorylated Cdc25A	Down	160	1.012E-02
p53-Independent DNA Damage Response	Down	160	1.012E-02
p53-Independent G1/S DNA damage checkpoint	Down	160	1.012E-02

mitochondrial fatty acid beta-oxidation of saturated fatty acids	Up	14	1.299E-02
UCH proteinases	Down	293	1.385E-02
APC/C:Cdc20 mediated degradation of Securin	Down	165	1.385E-02
Regulation of TNFR1 signalling	Down	421	1.547E-02
NOD1/2 signalling Pathway	Down	285	1.662E-02
APC/C:Cdh1 mediated degradation of Cdc20 and other APC/C:Cdh1 targeted proteins in late mitosis/early G1	Down	222	1.782E-02
Selective autophagy	Down	879	1.782E-02
TGF-beta receptor signalling activates SMADs	Down	318	1.810E-02
Anchoring fibril formation	Down	31	1.810E-02
Deubiquitination	Down	1227	1.810E-02
Cristae formation	Up	82	1.810E-02
Axon guidance	Down	1070	1.854E-02
Chaperone Mediated Autophagy	Down	769	1.854E-02
CLEC7A (Dectin-1) signalling	Down	358	1.858E-02
SCF-beta-TrCP mediated degradation of Emi1	Down	196	1.902E-02
PI3K/AKT signalling in Cancer	Down	540	1.949E-02
Pyruvate metabolism and Citric Acid (TCA) cycle	Up	99	1.955E-02
Respiratory electron transport, ATP synthesis by chemiosmotic coupling, and heat production by uncoupling proteins.	Up	227	2.024E-02
Nef Mediated CD4 Down-regulation	Down	51	2.061E-02
Crosslinking of collagen fibrils	Down	40	2.061E-02
TNF signalling	Down	457	2.122E-02
Activation of AMPK downstream of NMDARs	Down	95	2.124E-02
CDK-mediated phosphorylation and removal of Cdc6	Down	175	2.136E-02
Nervous system development	Down	1108	2.161E-02
Interleukin-1 signalling	Down	667	2.272E-02

Integrin cell surface interactions	Down	303	2.336E-02
Macroautophagy	Down	938	2.363E-02
Formation of ATP by chemiosmotic coupling	Up	25	2.363E-02
Regulation of activated PAK-2p34 by proteasome mediated degradation	Down	158	2.363E-02
Degradation of DVL	Down	184	2.363E-02
COPI-independent Golgi-to-ER retrograde traffic	Down	89	2.485E-02
Activation of NF-kappaB in B cells	Down	256	2.485E-02
SCF(Skp2)-mediated degradation of p27/p21	Down	221	2.576E-02
RHOQ GTPase cycle	Down	725	2.745E-02
Hh mutants abrogate ligand secretion	Down	182	2.869E-02
mRNA Capping	Down	70	3.175E-02
PI5P, PP2A and IER3 Regulate PI3K/AKT signalling	Down	533	3.213E-02
AUF1 (hnRNP D0) binds and destabilizes mRNA	Down	271	3.280E-02
Nuclear signalling by ERBB4	Down	325	3.313E-02
RHO GTPase Effectors	Down	1077	3.462E-02
Translocation of ZAP-70 to Immunological synapse	Down	22	3.481E-02
Hh mutants are degraded by ERAD	Down	181	3.559E-02
APC:Cdc20 mediated degradation of cell cycle proteins prior to satisfaction of the cell cycle checkpoint	Down	186	3.638E-02
GSK3B and BTRC:CUL1-mediated-degradation of NFE2L2	Down	211	3.756E-02
TNFR2 non-canonical NF-kB pathway	Down	308	3.783E-02
Metabolism of proteins	Down	2358	3.787E-02
Cdc20:Phospho-APC/C mediated degradation of Cyclin A	Down	185	3.960E-02
Degradation of AXIN	Down	176	3.960E-02
Asymmetric localization of PCP proteins	Down	176	4.030E-02
TP53 regulates transcription of additional cell cycle genes whose exact role in the p53 pathway remain uncertain	Down	118	4.047E-02

Hedgehog ligand biogenesis	Down	200	4.048E-02
Orc1 removal from chromatin	Down	211	4.079E-02
Switching of origins to a post-replicative state	Down	230	4.137E-02
Activation of APC/C and APC/C:Cdc20 mediated degradation of mitotic proteins	Down	210	4.137E-02
Negative regulation of the PI3K/AKT network	Down	549	4.137E-02
APC/C:Cdc20 mediated degradation of mitotic proteins	Down	187	4.137E-02
Autophagy	Down	988	4.171E-02
Membrane Trafficking	Down	1582	4.321E-02
Regulation of APC/C activators between G1/S and early anaphase	Down	249	4.389E-02
APC/C-mediated degradation of cell cycle proteins	Down	275	4.444E-02
Regulation of mitotic cell cycle	Down	275	4.444E-02
Transcriptional regulation by RUNX1	Down	625	4.521E-02
Death Receptor signalling	Down	686	4.731E-02
ALK mutants bind TKIs	Down	72	4.731E-02
Somitogenesis	Down	165	4.942E-02
Vesicle-mediated transport	Down	1633	4.989E-02

Figure Descriptors:

Figure 1: Clinically compatible cachexia profile of mice treated with anti-acute myeloid leukemia (AML) chemotherapy. Pre- to post-treatment changes in (A) body mass and composition of lean and fat mass. (B) Average daily food intake over the treatment protocol. (C) Effect of treatment on endpoint muscle and tissue mass and on (D) tibialis anterior (TA) fibre size distribution, mean fibre size and representative H&E-stained images. (E) Protein expression of fast and slow myosin heavy chain (MHC) isoforms and traditional atrophy signalling markers, Atrogin-1 (Fbxo32), TGFβ-myostatin-Smad axis, and Murf-1 (Trim63). (F) Collagen content and representative picrosirius stained images of TA. *p<0.05, **p<0.01, ***p<0.001, ****p<0.0001 CIR different from vehicle (VEH), #p<0.05, ##p<0.01 main CIR effect. Scale bar for H&E images = 50 µm; for picrosirius images = 200 µm.

Figure 2: Physical activity and whole-body metabolism are reduced in mice treated with acute myeloid leukemia (AML) chemotherapy induction regimen (CIR). Mice were assessed continuously for (A) cage ambulatory distance and (B) energy expenditure, which is expressed relative to day 1 levels. (C) Start- and end-point energy expenditure (kcal) expressed relative to lean tissue mass and (D) the respiratory quotient (VCO_2/VO_2) are shown. Data are mean ± SEM. *p<0.005, **p<0.01, ***p<0.001 CIR versus vehicle (VEH).

Figure 3: Muscle proteome response to acute myeloid leukemia (AML) chemotherapy induction regimen (CIR) reveals haptoglobin (Hp) and glutamine synthetase (Glul) as potential biomarkers. (A) Volcano plot showing upregulation of Hp and Glul. (B) heatmap of individual mouse muscle expression of Hp and Glul. (C) Significantly upregulated Reactome pathways. (D) Protein expression profile of branched chain amino acid (BCAA) catabolism, and β-fat oxidation, mitochondrial tricarboxylic acid (TCA) cycle and mitochondrial complex I (mit-CI) metabolism Reactome pathways. (E) Uncoupling-related protein expression. (F) top 25 downregulated Reactome pathways in response to AML CIR treatment. *p<0.05, **p<0.01, ***p<0.001, ****p<0.0001 CIR versus vehicle (VEH).

Figure 4: Recovery profile following of acute myeloid leukemia (AML) chemotherapy induction regimen (CIR). (A) Experimental timeline. (B) Body mass over the AML CIR and recovery time course. (C) Body, lean and fat mass displacement relative to vehicle (VEH) over the recovery time course. (D) Endpoint muscle mass of the extensor digitorum longus (EDL), soleus (SOL) and tibialis anterior (TA). (E) Volcano plot of unresponsive

quadriceps muscle proteome to CIR cessation after two weeks. (F) Haptoglobin (Hp) and glutamine synthetase (Glul) expression at the treatment (CIR) and recovery (CIR RECOV) endpoints for individual animals. *p<0.05, **p<0.01, ****p<0.0001 CIR RECOV relative to age-matched VEH; #p<0.05, ####p<0.0001 main group effect; ^p<0.05, ^^p<0.01 within group time effect.

Figure 5: Worsening of cachexic fat mass loss by voluntary exercise during acute myeloid leukemia (AML) chemotherapy induction regimen (CIR) treatment further upregulates muscle haptoglobin (Hp) expression. (A) Voluntary physical activity (wheel running) reduces over the AML CIR treatment period alongside (B) reduced total energy expenditure. (C) Daily food intake and (D) change in body, lean and fat mass over the treatment period. (E) Mean tibialis anterior fibre size and (F) quadriceps proteome response to voluntary exercise in vehicle (VEH) and CIR treated mice, including reduction of uncoupling protein (Ucp) expression. *p<0.05, **p<0.01, ***p<0.001 active (ACT) versus sedentary (SED) and CIR versus VEH ACT; #p<0.05, ##p<0.01 main treatment effect.

Figure 6: Biomarker potential of muscle haptoglobin (Hp) and glutamine synthetase (Glul) in the context of acute myeloid leukemia (AML) chemotherapy induction regimen (CIR) cachexia. (A) Conditional heatmap signatures of Hp, Glul, Fbxo32 (Atrogin-1) and Trim63 (Murf-1) in AML CIRL and vehicle (VEH) treated muscles. Correlations of (B) Hp and (C) Glul expression with each other and with change in body, lean, fat mass. Grey dots/regression lines denote data points from VEH and CIR groups under all conditions, red data points/regression lines denote VEH and CIR recovery data points removed.

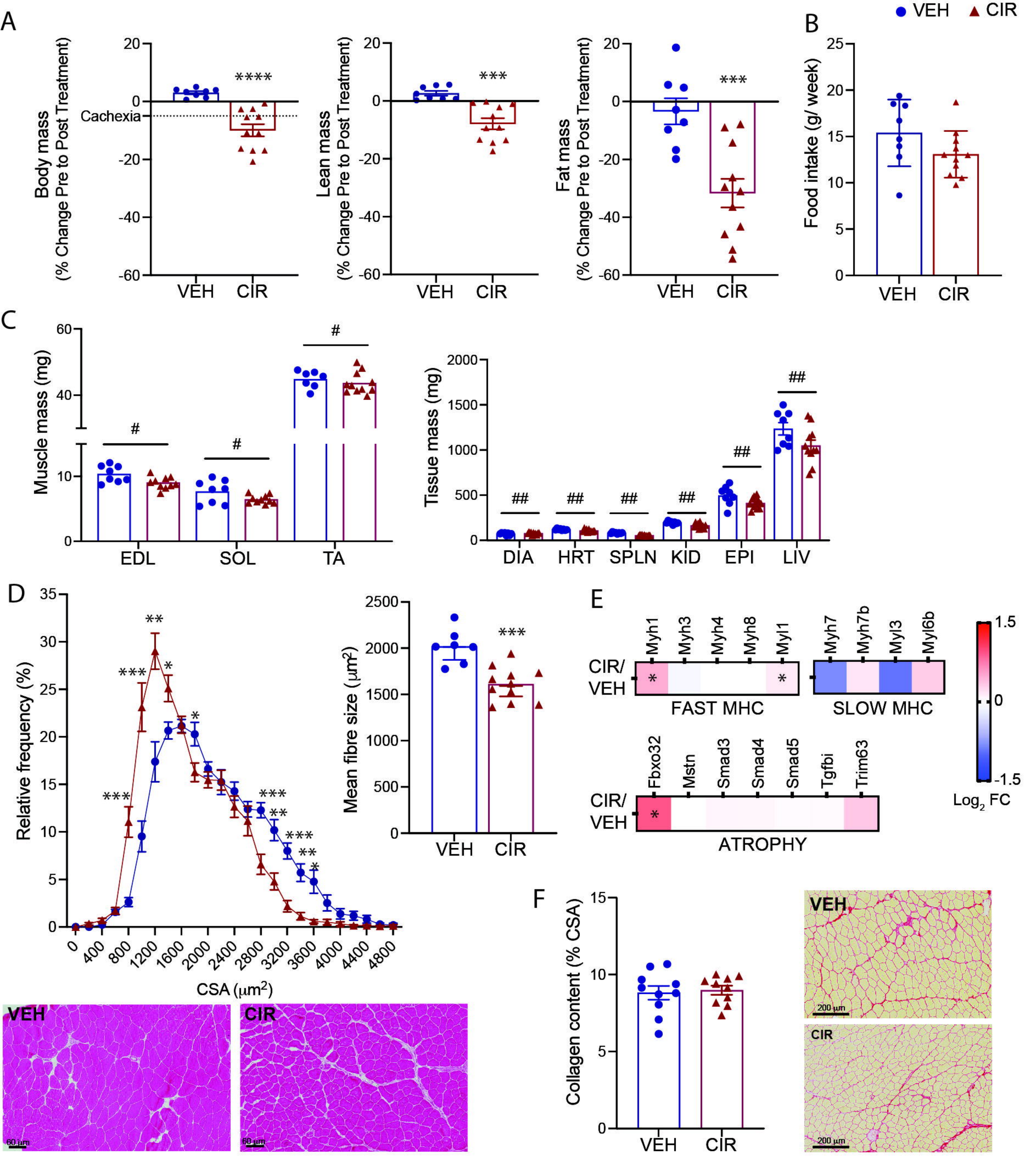
A
Body mass (% Change Pre to Post Treatment)
Cachexia
****
Lean mass (% Change Pre to Post Treatment)
***
Fat mass (% Change Pre to Post Treatment)
***
VEH
CIR
B
VEH
CIR
Food intake (g/ week)
C
Muscle mass (mg)
EDL
SOL
TA
Tissue mass (mg)
DIA
HRT
SPLN
KID
EPI
LIV
D
Relative frequency (%)
CSA (μm²)
Mean fibre size (μm²)
E
Myh1
Myh3
Myh4
Myh8
Myl1
Myh7
Myh7b
Myl3
Myl6b
CIR/ VEH
FAST MHC
SLOW MHC
Fbxo32
Mstn
Smad3
Smad4
Smad5
Tgfbi
Trim63
ATROPHY
Log₂ FC
F
Collagen content (% CSA)
VEH
CIR
200 μm
60 μm

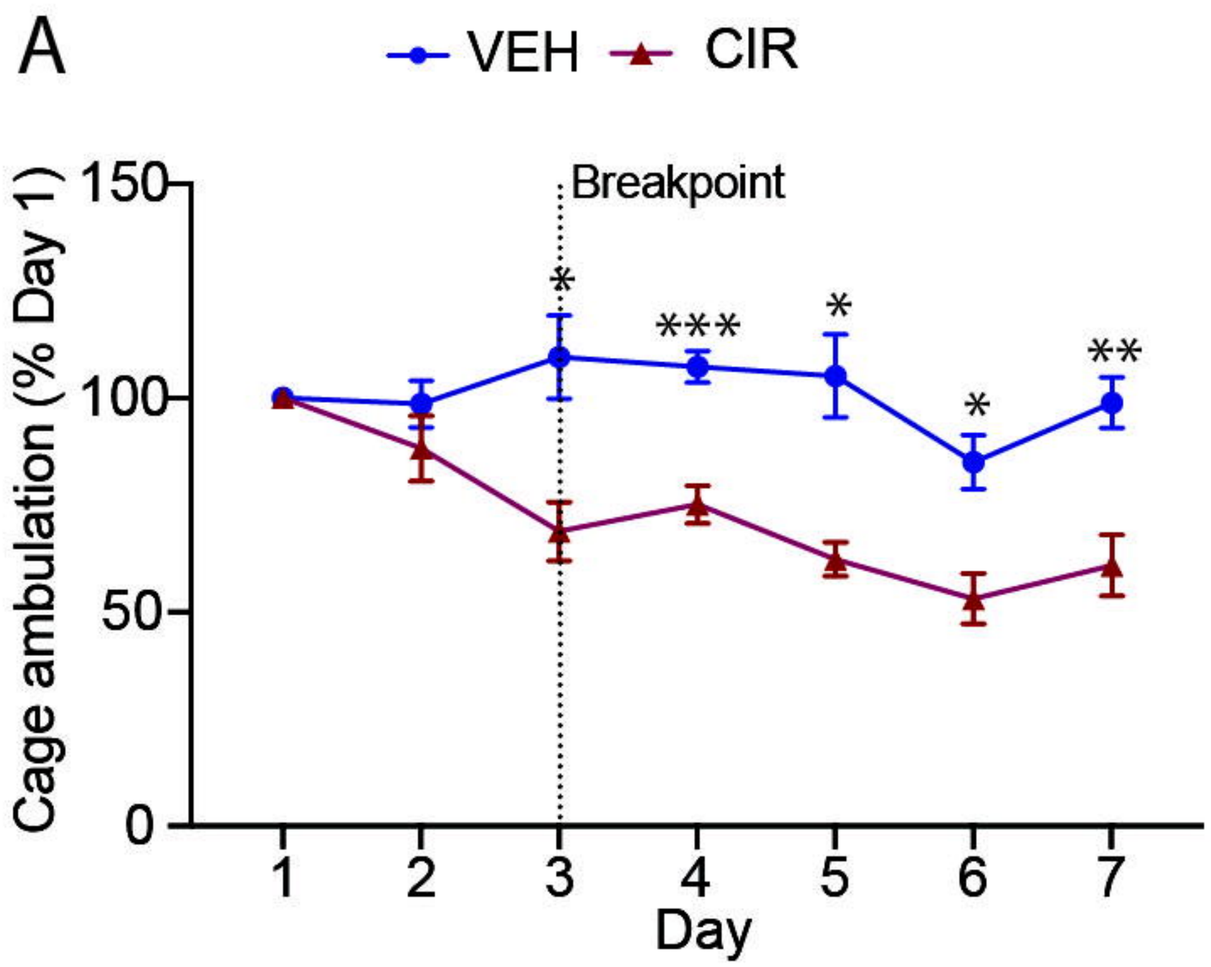
A
VEH
CIR
Breakpoint
Cage ambulation (% Day 1)
150
100
50
0
*
***
*
*
**
1
2
3
4
5
6
7
Day

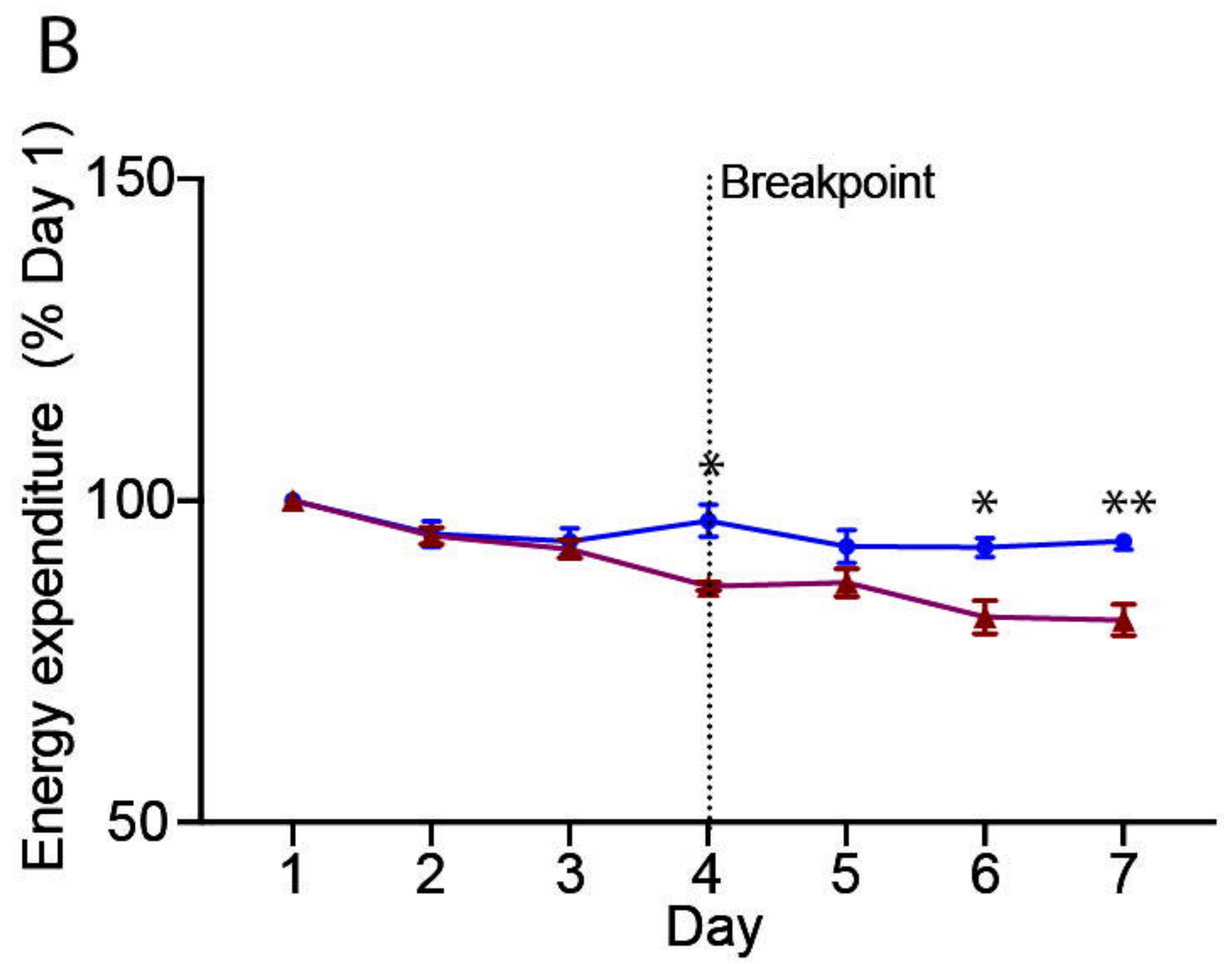
B
Breakpoint
Energy expenditure (% Day 1)
150
100
50
*
*
**
1
2
3
4
5
6
7
Day

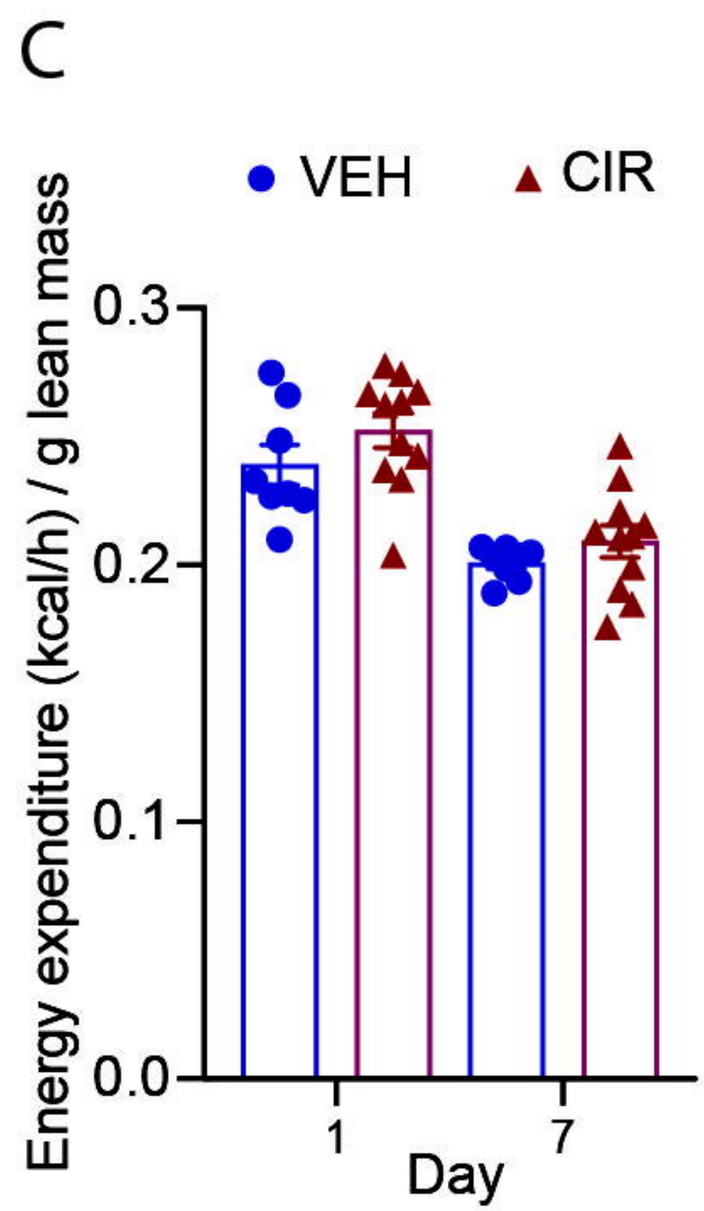
C
VEH
CIR
Energy expenditure (kcal/h) / g lean mass
0.3
0.2
0.1
0.0
1
7
Day

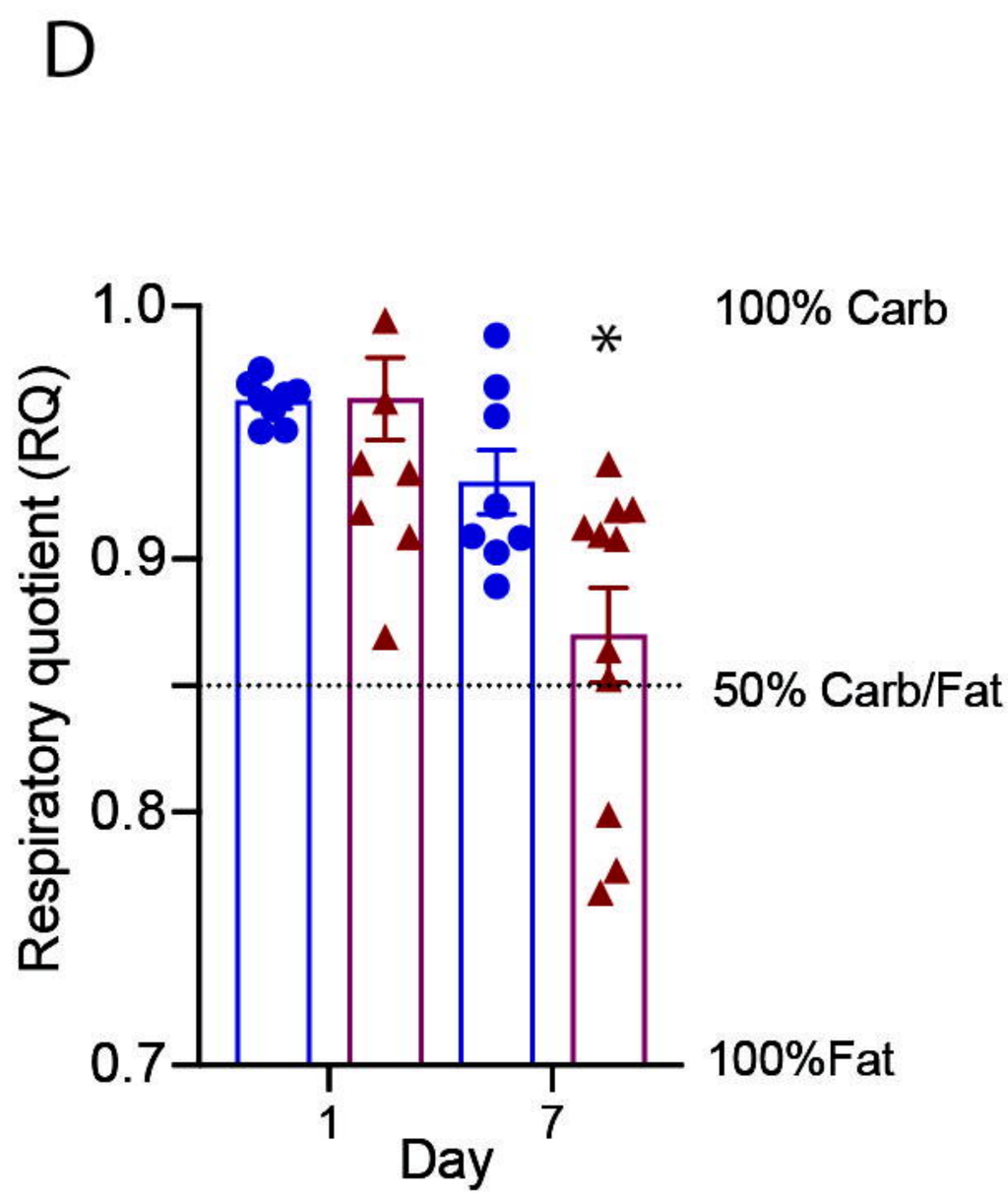
D
Respiratory quotient (RQ)
1.0
0.9
0.8
0.7
*
100% Carb
50% Carb/Fat
100%Fat
1
7
Day

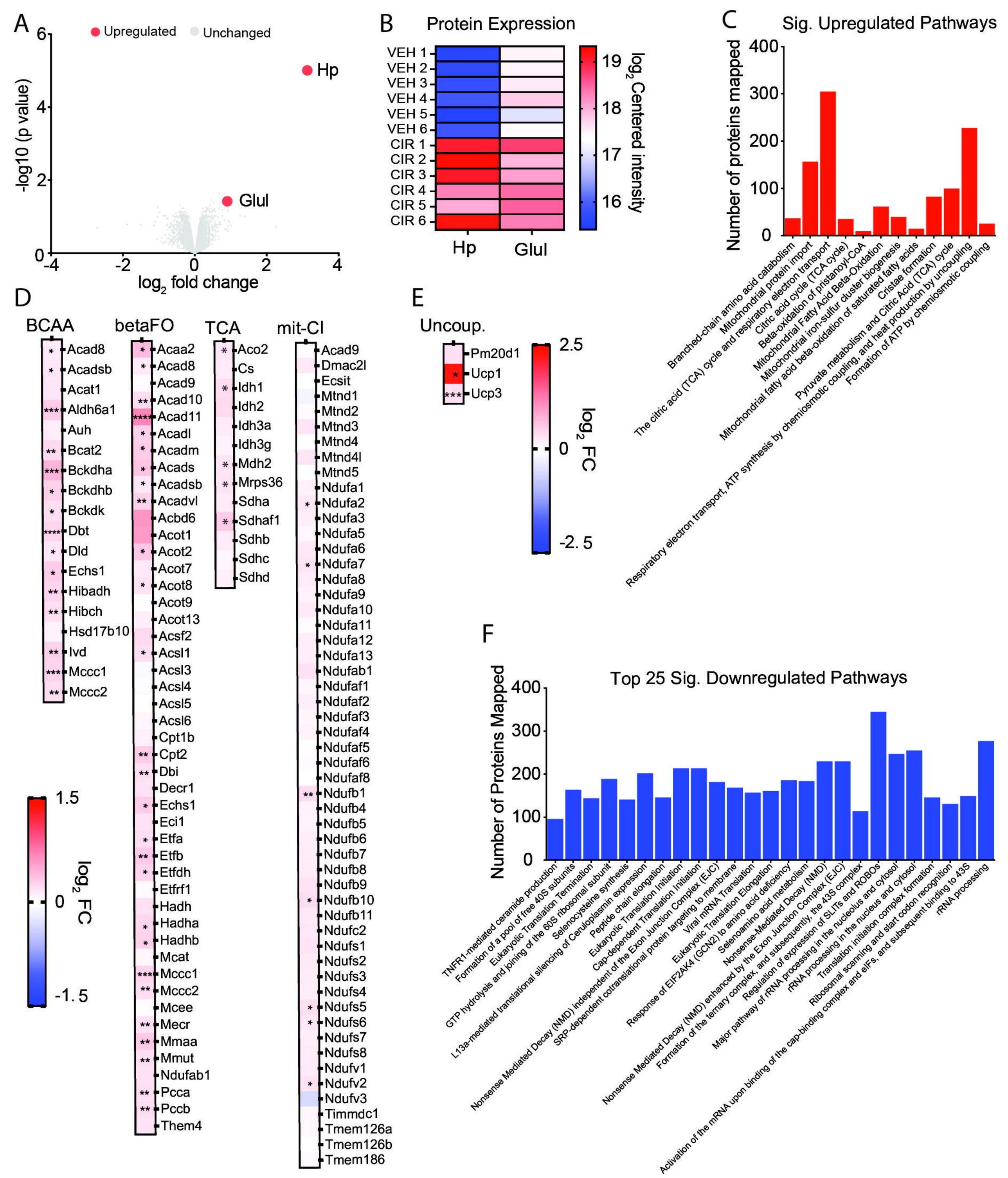
A
Upregulated
Unchanged
Hp
Glul
-log10 (p value)
log2 fold change
B
Protein Expression
VEH 1
VEH 2
VEH 3
VEH 4
VEH 5
VEH 6
CIR 1
CIR 2
CIR 3
CIR 4
CIR 5
CIR 6
Hp
Glul
log2 Centered intensity
C
Sig. Upregulated Pathways
Number of proteins mapped
Branched-chain amino acid catabolism
Mitochondrial protein import
Mitochondrial electron transport
The citric acid (TCA) cycle and respiratory electron transport
Citric acid cycle (TCA cycle)
Beta-oxidation of pristanoyl-CoA
Beta-Oxidation
Mitochondrial Fatty Acid Beta-Oxidation
Mitochondrial iron-sulfur cluster biogenesis
Mitochondrial fatty acid beta-oxidation of saturated fatty acids
Cristae formation
Pyruvate metabolism and Citric Acid (TCA) cycle
Respiratory electron transport, ATP synthesis by chemiosmotic coupling, and heat production by uncoupling
Formation of ATP by chemiosmotic coupling
D
BCAA
betaFO
TCA
mit-CI
log2 FC
E
Uncoup.
Pm20d1
Ucp1
Ucp3
log2 FC
F
Top 25 Sig. Downregulated Pathways
Number of Proteins Mapped
TNFR1-mediated ceramide production
Formation of a pool of free 40S subunits
Eukaryotic Translation Termination
GTP hydrolysis and joining of the 60S ribosomal subunit
L13a-mediated translational silencing of Ceruloplasmin expression
Selenocysteine synthesis
Peptide chain elongation
Eukaryotic Translation Initiation
Cap-dependent Translation Initiation
Nonsense Mediated Decay (NMD) independent of the Exon Junction Complex (EJC)
SRP-dependent cotranslational protein targeting to membrane
Viral mRNA Translation
Eukaryotic Translation Elongation
Response of EIF2AK4 (GCN2) to amino acid deficiency
Selenoamino acid metabolism
Nonsense-Mediated Decay (NMD)
Nonsense Mediated Decay (NMD) enhanced by the Exon Junction Complex (EJC)
Formation of the ternary complex, and subsequently, the 43S complex
Regulation of expression of SLITs and ROBOs
Major pathway of rRNA processing in the nucleolus and cytosol
rRNA processing in the nucleus and cytosol
Translation initiation complex formation
Ribosomal scanning and start codon recognition
Activation of the mRNA upon binding of the cap-binding complex and eIFs, and subsequent binding to 43S
rRNA processing

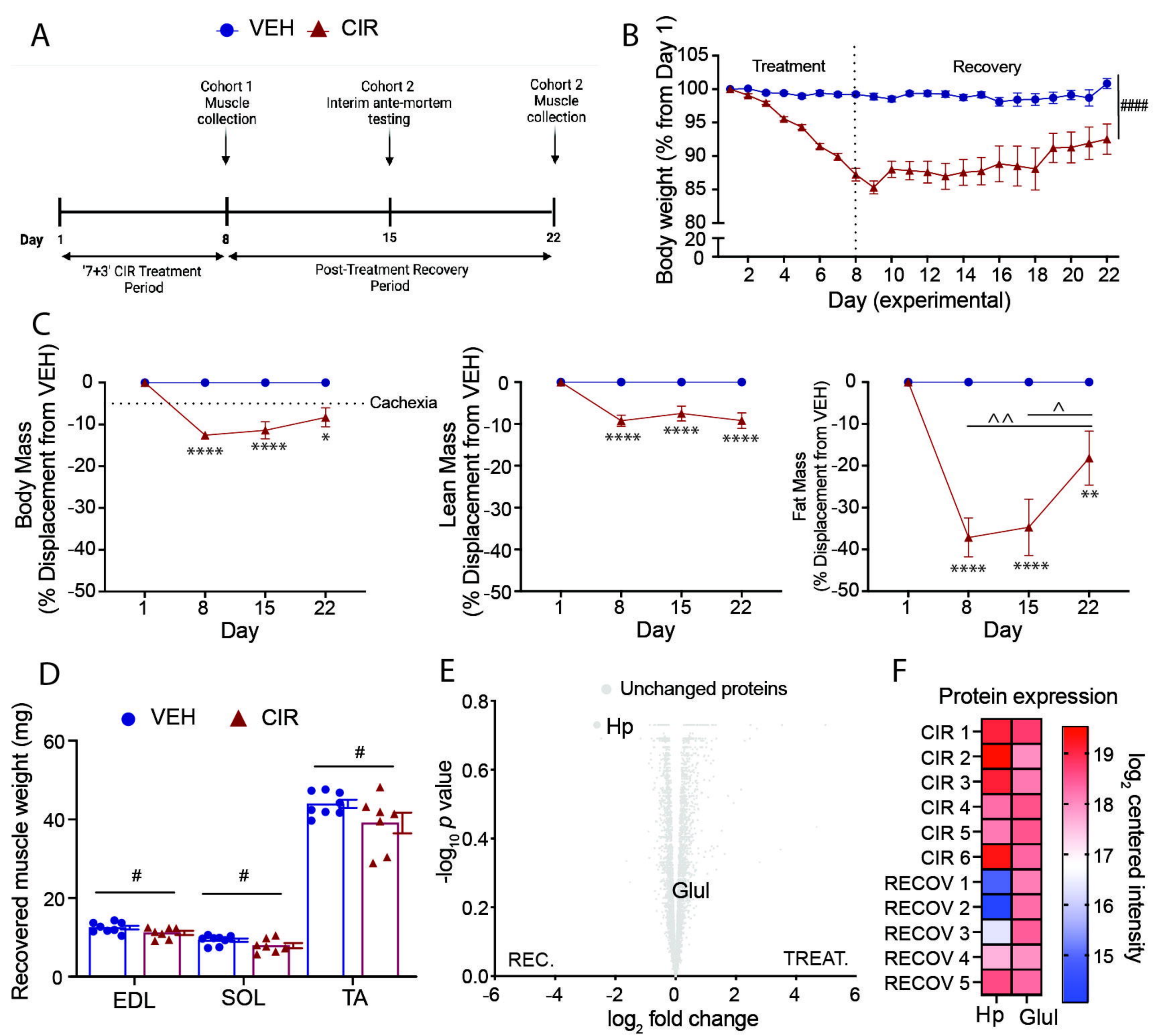
A
VEH
CIR
Cohort 1 Muscle collection
Cohort 2 Interim ante-mortem testing
Cohort 2 Muscle collection
Day
1
8
15
22
'7+3' CIR Treatment Period
Post-Treatment Recovery Period
B
Treatment
Recovery
Body weight (% from Day 1)
Day (experimental)
####
C
Body Mass (% Displacement from VEH)
Cachexia
Lean Mass (% Displacement from VEH)
Fat Mass (% Displacement from VEH)
Day
D
VEH
CIR
Recovered muscle weight (mg)
EDL
SOL
TA
E
Unchanged proteins
Hp
Glul
REC.
TREAT.
-log10 p value
log2 fold change
F
Protein expression
CIR 1
CIR 2
CIR 3
CIR 4
CIR 5
CIR 6
RECOV 1
RECOV 2
RECOV 3
RECOV 4
RECOV 5
Hp
Glul
log2 centered intensity

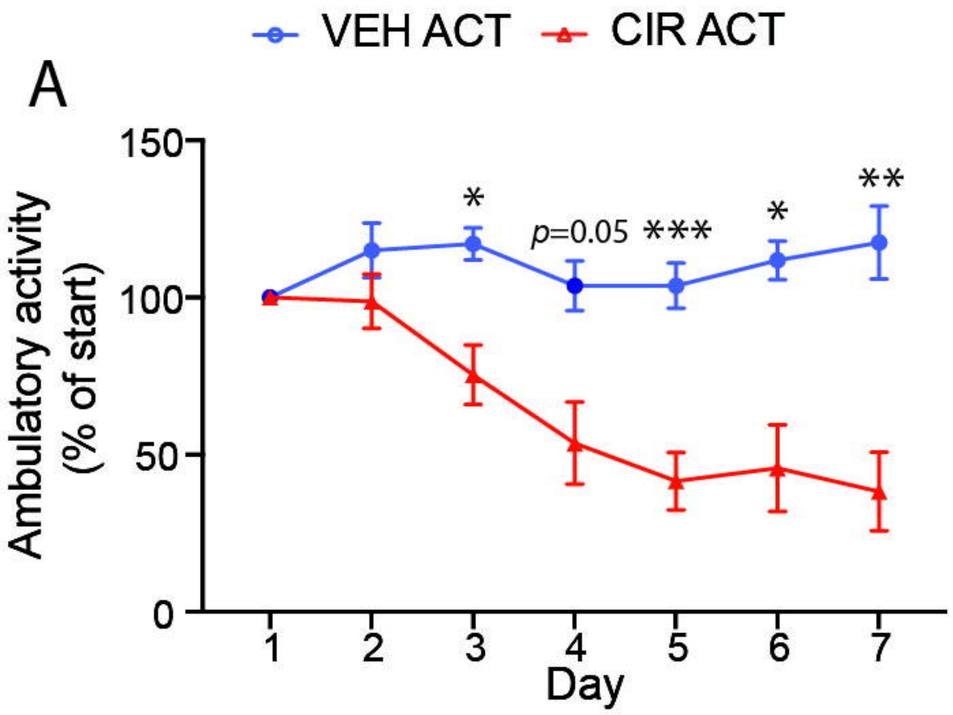

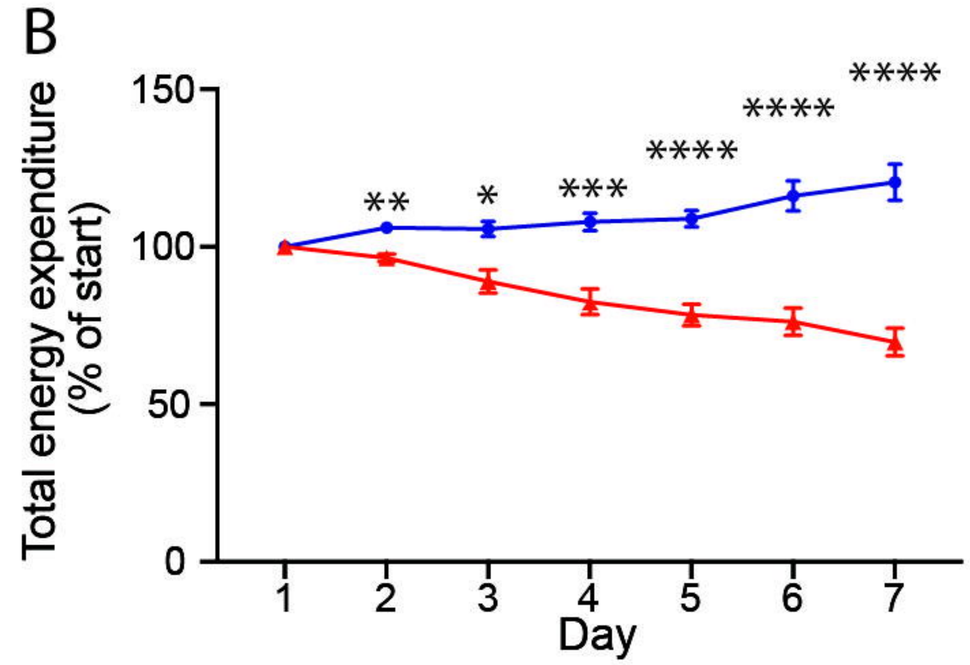

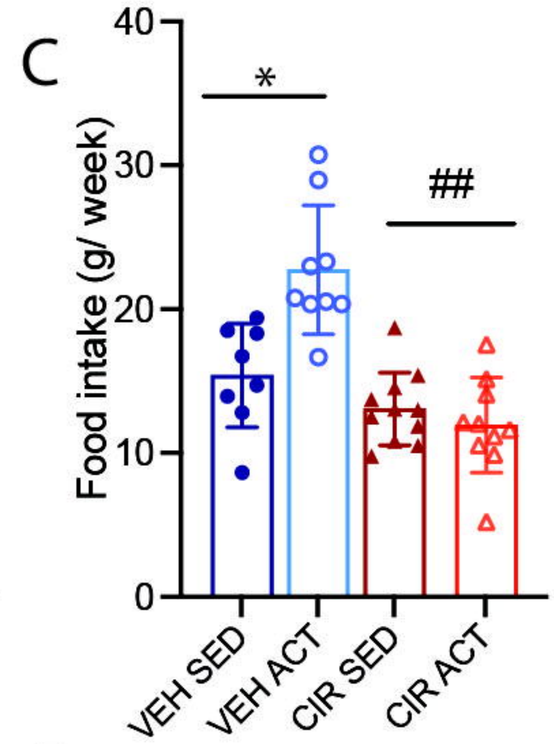

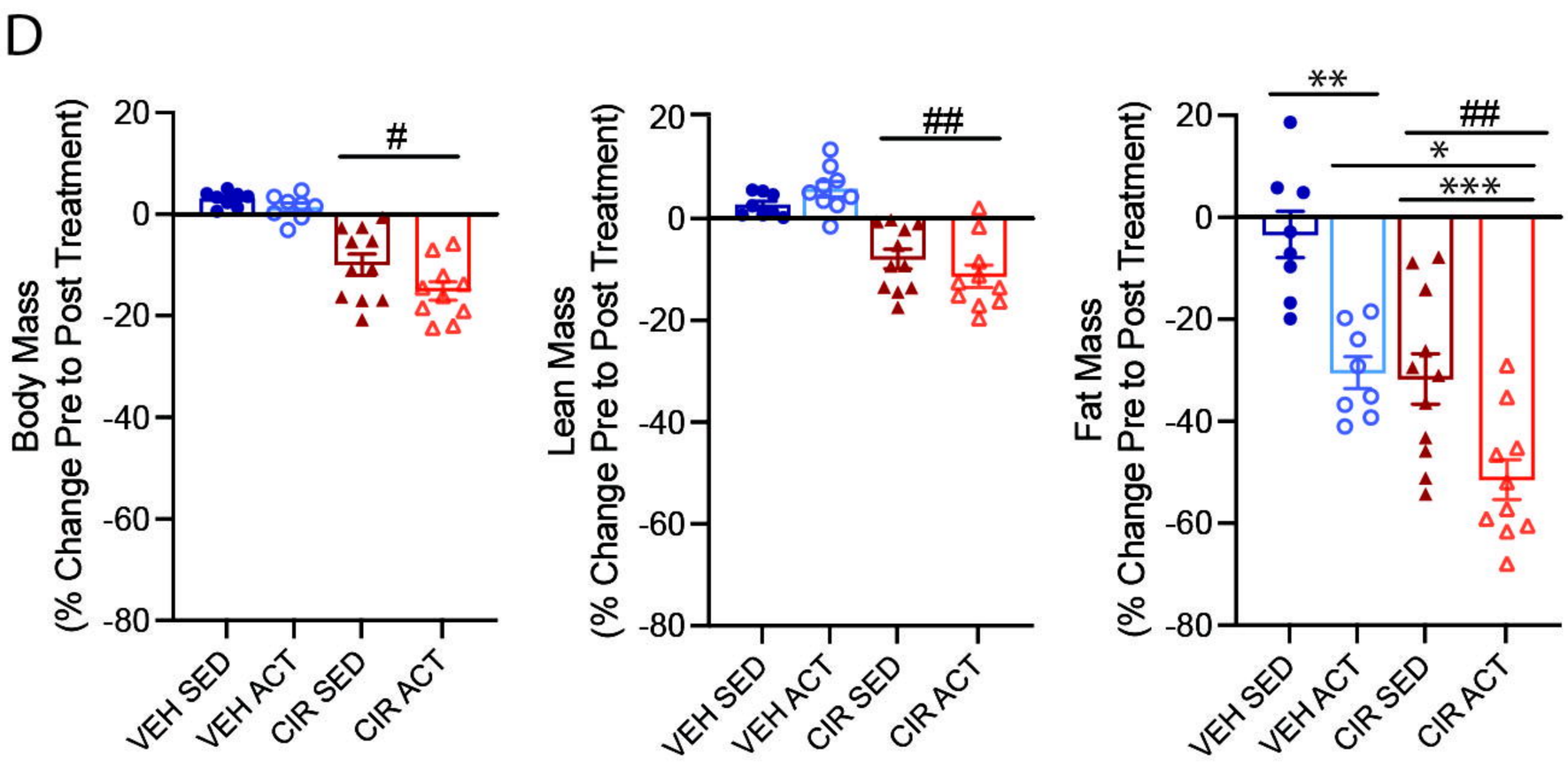

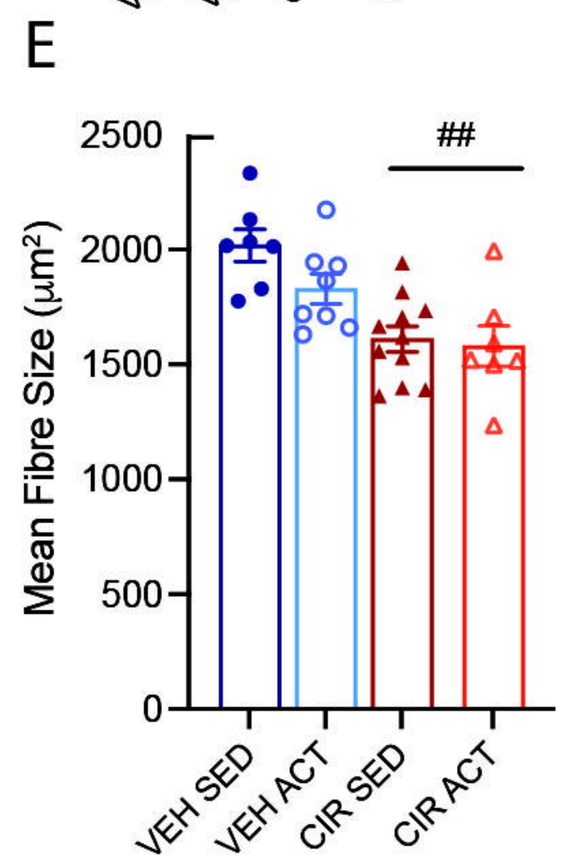

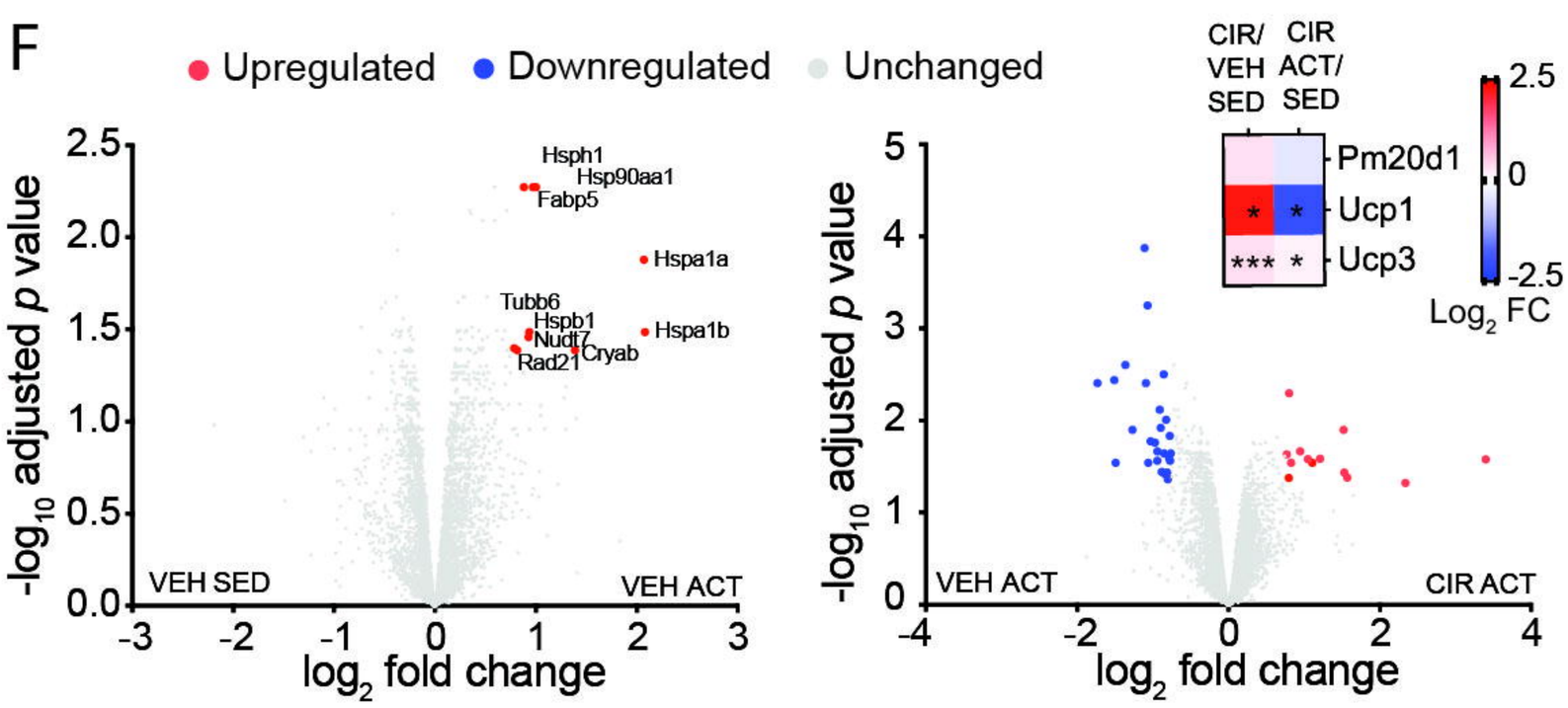

Protein	Log₂ Fold Change	-log₁₀ adjusted *p* value	Protein	Log₂ Fold Change	-log₁₀ adjusted *p* value
Hp	3.4	1.576	Plod1	-0.824	2.007
Myl3	2.34	1.323	Gypa	-0.846	1.425
Pdk4	1.57	1.379	Pi16	-0.849	1.643
Serpina3m	1.53	1.436	Rrbp1	-0.857	2.501
Plin5	1.52	1.899	Smox	-0.881	1.442
Myoz2	1.21	1.585	C8b	-0.896	1.920
Apcs	1.11	1.543	Ckap4	-0.91	2.116
Retreg1	1.05	1.583	Apoc1	-0.939	1.562
Inmt	0.951	1.665	Aplp2	-0.94	1.665
Myh7b	0.829	1.543	Pcolce	-0.97	1.761
Lrrc2	0.802	2.297	P4ha1	-1.03	1.774
Cwc22	0.797	1.378	Ear2	-1.06	1.543
Slmap	0.769	1.632	Fkbp10	-1.07	3.249
C8g	-0.764	1.643	C9	-1.09	2.406
Pxdn	-0.773	1.563	Serpinh1	-1.11	3.872
C8a	-0.774	1.835	Rcn3	-1.27	1.899
Gfpt2	-0.783	1.593	Lifr	-1.36	2.605
Aacs	-0.798	1.375	Igfbp5	-1.49	1.543
H2Ab1	-0.804	1.363	Mup3	-1.51	2.440
Lsp1	-0.809	1.436	Mup2	-1.73	2.406

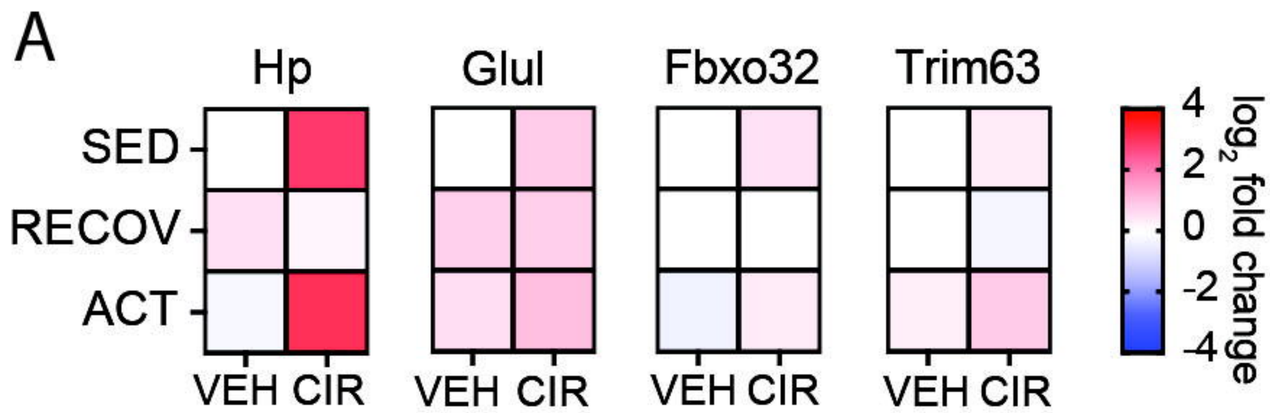
A
Hp
Glul
Fbxo32
Trim63
SED
RECOV
ACT
VEH CIR
VEH CIR
VEH CIR
VEH CIR
4
2
0
-2
-4
log2 fold change

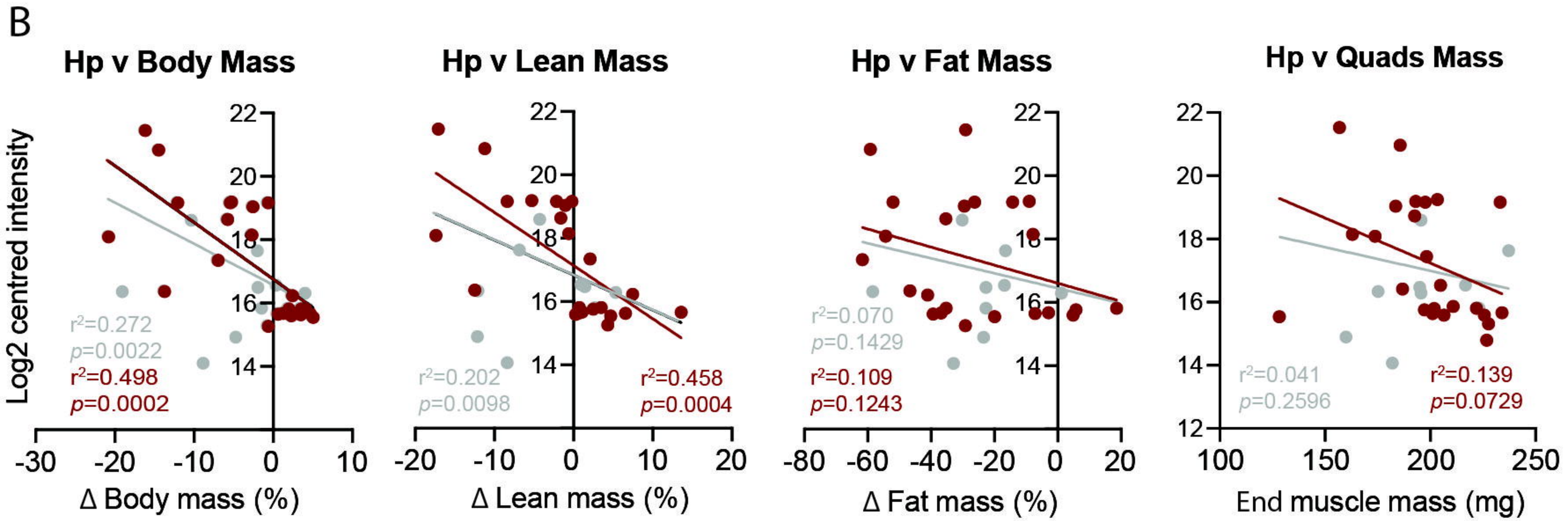
B
Hp v Body Mass
Hp v Lean Mass
Hp v Fat Mass
Hp v Quads Mass
Log2 centred intensity
r²=0.272
p=0.0022
r²=0.498
p=0.0002
r²=0.202
p=0.0098
r²=0.458
p=0.0004
r²=0.070
p=0.1429
r²=0.109
p=0.1243
r²=0.041
p=0.2596
r²=0.139
p=0.0729
Δ Body mass (%)
Δ Lean mass (%)
Δ Fat mass (%)
End muscle mass (mg)

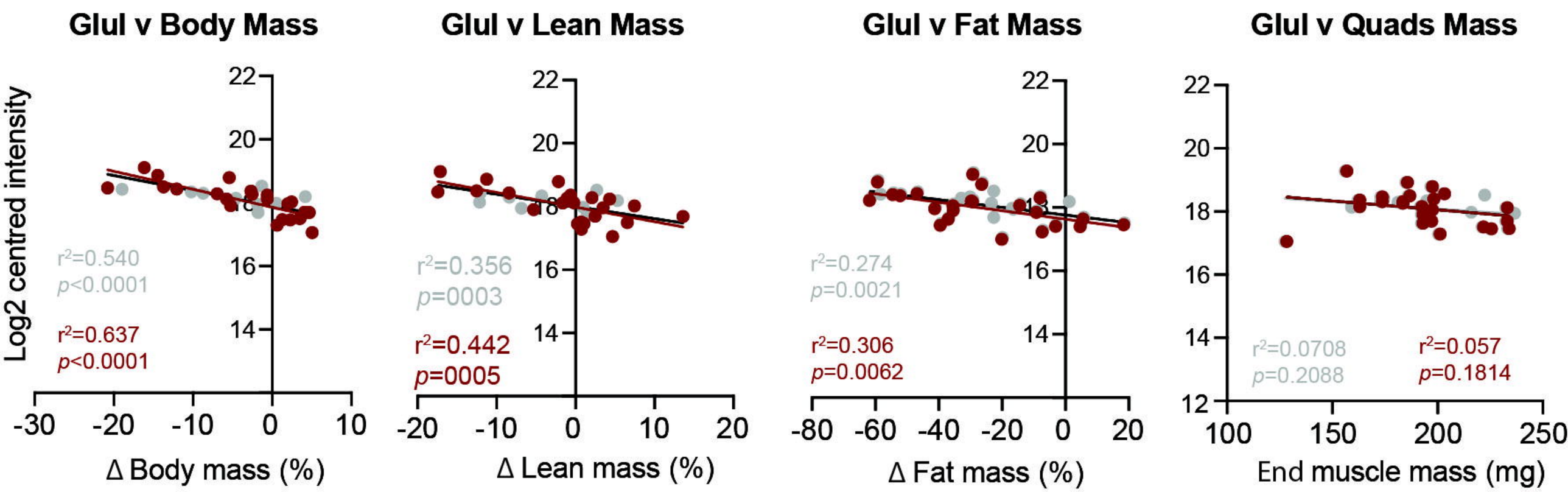
C
Glul v Body Mass
Glul v Lean Mass
Glul v Fat Mass
Glul v Quads Mass
Log2 centred intensity
r²=0.540
p<0.0001
r²=0.637
p<0.0001
r²=0.356
p=0003
r²=0.442
p=0005
r²=0.274
p=0.0021
r²=0.306
p=0.0062
r²=0.0708
p=0.2088
r²=0.057
p=0.1814
Δ Body mass (%)
Δ Lean mass (%)
Δ Fat mass (%)
End muscle mass (mg)